GERMAN - MONGOLIAN INSTITUTE FOR RESOURCES AND TECHNOLOGY

The present work was submitted to
the German-Mongolian Institute of Resources and Technology

DESIGN AND SIMULATION OF A TEMPERATURE-CONTROLLED VENTILATION SYSTEM FOR A GREENHOUSE

Bachelor Thesis

by

ERDENEJARGAL Boldbaatar

Study program: Mechatronics Engineering

Student ID: B2200236

Supervisor 1 / Examiner 1 **Prof. Odbileg Norov**

Supervisor 2 / Examiner 2 **Phd. Kim Young Suk**

Ulaanbaatar/Nalaikh,
2026

GERMAN - MONGOLIAN INSTITUTE FOR RESOURCES AND TECHNOLOGY

The present work was submitted to
the German-Mongolian Institute of Resources and Technology

DESIGN AND SIMULATION OF A TEMPERATURE-CONTROLLED VENTILATION SYSTEM FOR A GREENHOUSE

Bachelor Thesis

by

ERDENEJARGAL Boldbaatar

Study program: Mechatronics Engineering

Student ID: B2200236

Supervisor 1 / Examiner 1 **Prof. Odbileg Norov**

Supervisor 2 / Examiner 2 **Phd. Kim Young Suk**

Ulaanbaatar/Nalaikh,
2026

Statutory Declaration

Boldbaatar Erdenejargal	B2200236
Last Name, First Name	Student ID Number

I hereby affirm in lieu of an oath that I provided the submitted bachelor thesis

"Design And Simulation Of A Temperature-Controlled Ventilation System For A Greenhouse"

I did not use any sources other than those stated. In case that the work is additionally submitted on a data medium, I declare that the written and the electronic form are completely identical. The work was not submitted in the same or similar form to any examination authority.

Place, Date	Signature

ACKNOWLEDGEMENT

I would like to express my gratitude to Prof.Odbileg Norov and Kim Young Suk, for accepting to be my supervisors, and my providing me with advice and direction.
I thank my family and friends for their constant support and encouragement.
Finally, I acknowledge the perseverance and dedication required to complete this research during challenging periods.

ABSTRACT

This thesis presents the engineering design of a temperature-controlled forced ventilation greenhouse system adapted to the continental semi-arid climate of Ulaanbaatar, Mongolia. The study follows a dual methodology: a parametric three-dimensional structural model developed in Autodesk Inventor 2026, and a discrete-time PID temperature controller implemented and verified within the Wokwi embedded systems simulator. A thermal load analysis, using a peak solar irradiance of 800 W/m² and an ambient design temperature of 35°C, established a peak solar heat gain of 58.3 kW for a single-span greenhouse of 189 m³ internal volume clad in 16 mm twin-wall polycarbonate. The resulting design ventilation rate of 30 air changes per hour corresponds to a volumetric flow of 1.57 m³/s, delivered by a North-wall intake fan through a three-branch perforated PVC duct network. Perforation spacing is tapered from 300 mm at the inlet to 200 mm at the capped end, following the Teitel hydraulic pressure-compensation model, to promote uniform jet discharge across the full branch length. The PID controller was tuned using the Ziegler–Nichols closed-loop method, yielding gains of Kp = 4.8, Ki = 0.16, and Kd = 36.0. Four simulation scenarios step response, setpoint tracking, disturbance rejection, and anti-windup verification confirmed all twelve specified control behaviors, including proportional fan modulation, integral setpoint convergence, derivative disturbance response, anti-windup clamping, and independent safety cutoff at 45°C. The thesis explicitly acknowledges that CFD spatial validation and physical hardware testing constitute the primary recommended continuation of this work.

Table of Contents

ACKNOWLEDGEMENT 1
ABSTRACT 1
1. INTRODUCTION 5
1.1 Background and Motivation 5
1.2 Problem Statement 6
1.3 Scope and Limitations 7
2. STATE OF THE ART 8
2.1. Greenhouse Thermal Environment 8
2.2. Greenhouse Thermal Modeling 8
2.3. Ventilation Systems in Greenhouses 10
2.3.1 Forced Mechanical Ventilation 11
2.3.2 Holed Duct Air Distribution Systems 12
2.4 CFD Simulation of Greenhouse Environments 13
2.4.1 Governing Equations 13
2.4.2 Turbulence Modelling 13
2.4.3 Boundary Conditions and Numerical Approach 14
2.4.4 Application to Forced Ventilation Greenhouses 14
2.5. Control Systems for Greenhouse Temperature 15
2.5.1 The Greenhouse as a Control Problem 15
2.5.2 Feedback Control Fundamentals 15
2.5.3 The PID Controller 16
2.5.4 Proportional Term 16
2.5.5 Integral Term 17
2.5.6 Derivative Term 17
2.5.7 PID Tuning Ziegler Nichols Method 17
2.5.8 Digital Implementation on Arduino 18
2.6 Research Gap and Thesis Positioning 19
2.6.1 Summary of Established Knowledge 19
2.6.2 Identified Gaps in the Literature 19
2.6.3 Thesis Positioning 20
2.6.4 Thesis Objectives 21
3. SYSTEM DESIGN 22
3.1 Chapter Overview 22
3.2 Greenhouse Context and Orientation 22
3.2.1 Site Context and Orientation 22
3.2.2 Geometric Parameters 23
3.2.3 Glazing Material 24

3.3 Thermal Load Analysis 25
3.3.1 Internal Volume and Glazed Area Calculation 25
3.3.2 Peak Solar Heat Gain 25
3.3.3 Required Ventilation Rate 25
3.4 Ventilation System Design 26
3.4.1 Fan Placement and Airflow Path 26
3.5 Perforated Duct Air Distribution System 27
3.5.1 Design Reasoning 27
3.5.2 Duct Layout and Dimensions 27
3.5.3 Perforation Spacing Tapering 29
3.5.4 Discharge Angle 30
3.6 Control System Design 30
3.6.1 System Overview 30
3.6.2 Signal Flow 32
3.6.3 Anti-Windup Implementation 32
3.6.4 User Interface 33
3.6.5 Sensor Specification and Limitation 33
3.7 Temperature Sensor Placement 33
4. MATERIALS AND METHODS 34
4.1 Chapter Overview 34
4.2 Greenhouse 3D Model Development 34
4.2.1 Geometry Construction in Autodesk Inventor 34
4.2.2 Ventilation Openings 34
4.2.3 Perforated Duct Network 34
4.3 Control System Implementation and Simulation 35
4.3.1 Simulation Environment 35
4.3.2 Simulated Circuit Configuration 35
4.3.3 Cooling System Control Action 37
4.3.4 PID Gain Values 37
4.3.5 Simulation Test Scenarios 38
4.3.6 Data Collection 38
5. RESULTS 39
5.1 Chapter Overview 39
5.2 PID Control System Simulation Results 39
5.2.1 Overview 39
5.2.2 Scenario 1: Step Response 39
5.2.3 Scenario 2: Setpoint Tracking 40
5.2.4 Scenario 3: Disturbance Rejection 42

5.2.5 Scenario 4: Anti-Windup Verification 43
5.2.6 Safety Cutoff Verification 44
5.2.7 Summary of Verified Control Behaviors 44
6. DISCUSSION / CONCLUSIONS 46
6.1 Summary of Engineering Work Completed 46
6.2 Limitations and Unmet Objectives 46
6.3 Recommendations for Continuation 47
6.4 Engineering Conclusions 48
References 48
Appendix: A 53

List of Figures

Figure 1-1. Seasonal Mean Temperature in Mongolia 7
Figure 2-1. Energy Balance in a Typical Greenhouse 9
Figure 2-2. Block Diagram of the Temperature Control System 16
Figure 2-3. Ziegler-Nichols Ultimate Gain method; Response with ultimate gain 18
Figure 3-1. Isometric View of Greenhouse Design 23
Figure 3-2. Isometric View of Duct System 28
Figure 3-3. Isometric View of Branch Duct 29
Figure 3-4. The KiCad schematic figure 31
Figure 4-1. The 3D Circuit Visualization generated by Wokwi 36
Figure 5-1. Serial Plotter, Scenario 1 40
Figure 5-2. Serial Plotter, Scenario 2 41
Figure 5-3. Serial Plotter, Scenario 3 42
Figure 5-4. Serial Plotter, Scenario 4 43
Figure 5-5. Red LED active at 45.4°C 44
Figure A-1. Final Assembly of a Greenhouse 53
Figure A-2. Arduino Source Code 55

1. INTRODUCTION

1.1 Background and Motivation

Global food production faces mounting pressure from a growing world population, declining arable land, and increasing climate variability. Controlled environment agriculture the practice of growing crops within enclosed structures where temperature, humidity, and light are actively regulated has emerged as one of the principal engineering responses to this challenge. The global controlled environment agriculture market was valued at USD 100.31 billion in 2023 and is projected to grow at a compound annual growth rate of 17.65% through 2033 [1], reflecting both the economic scale of the sector and the rate at which engineering investment in it is accelerating. Thermal behavior follows the same basic heat transfer principles in both high-tech Dutch glasshouses and low-cost single-span structures in developing regions.

Mongolia presents a particularly acute case for greenhouse technology adoption. Landlocked and far from the sea, Mongolia's vast grazing lands and harsh weather conditions impose short growing seasons that skew diets and can lead to malnutrition. [2] The reliance on rural livestock and rainfed agriculture, along with fragile ecosystems, puts Mongolia's economy at risk of adverse climate change impacts, particularly from extreme weather events. [3] To overcome these obstacles, Mongolia must utilize technology from crop genetics to greenhouses and aquaponics to achieve stability in food production for its citizens. [4] The greenhouse represents the most direct engineering pathway to year round vegetable production in a climate where outdoor growing is restricted to a narrow summer window and winter temperatures regularly fall below -30°C.

Greenhouse operation in continental climates is primarily a thermal management issue. The same glass structure that retains winter solar heat can cause extreme summer overheating, with internal temperatures reaching over 50°C even if outside is 30–35°C [1]. Maintaining optimal internal temperature requires real-time feedback control systems to adjust ventilation based on measured temperature changes. This challenge falls under mechatronics, integrating sensors, embedded controls, and thermal design.

1.2 Problem Statement

Temperature regulation in greenhouse forced ventilation systems presents three interconnected engineering challenges that motivate the present thesis.

The first challenge is physical design. A ventilation system must be sized and configured to deliver sufficient airflow to remove the peak solar heat load, and the air distribution network must introduce that airflow uniformly across the greenhouse volume rather than concentrating it at a single discharge point. Poor physical design an undersized fan, an absent duct distribution system, or a misplaced exhaust results in temperature gradients and hot zones that no amount of control sophistication can correct.

The second challenge is control system design. ON/OFF fan control, common in budget greenhouses, causes temperature swings due to its binary operation. A PID controller reduces these fluctuations by adjusting fan speed based on temperature error and its trends. Implementing PID on low-cost hardware demands careful gain tuning and attention to issues like sensor quantization and integral windup.

The third challenge is climate specificity. The overwhelming majority of published greenhouse CFD simulation and control system studies are conducted for temperate European, Mediterranean, or subtropical climates [3, 4]. The continental semi-arid climate of Ulaanbaatar, Mongolia with peak summer temperatures of 35°C, peak solar irradiance exceeding 800 W/m², and winter temperatures as low as -30°C imposes a uniquely demanding thermal design brief that is essentially absent from the published literature. Design decisions appropriate for a mild temperate climate may be inadequate or incorrect for the Mongolian context.

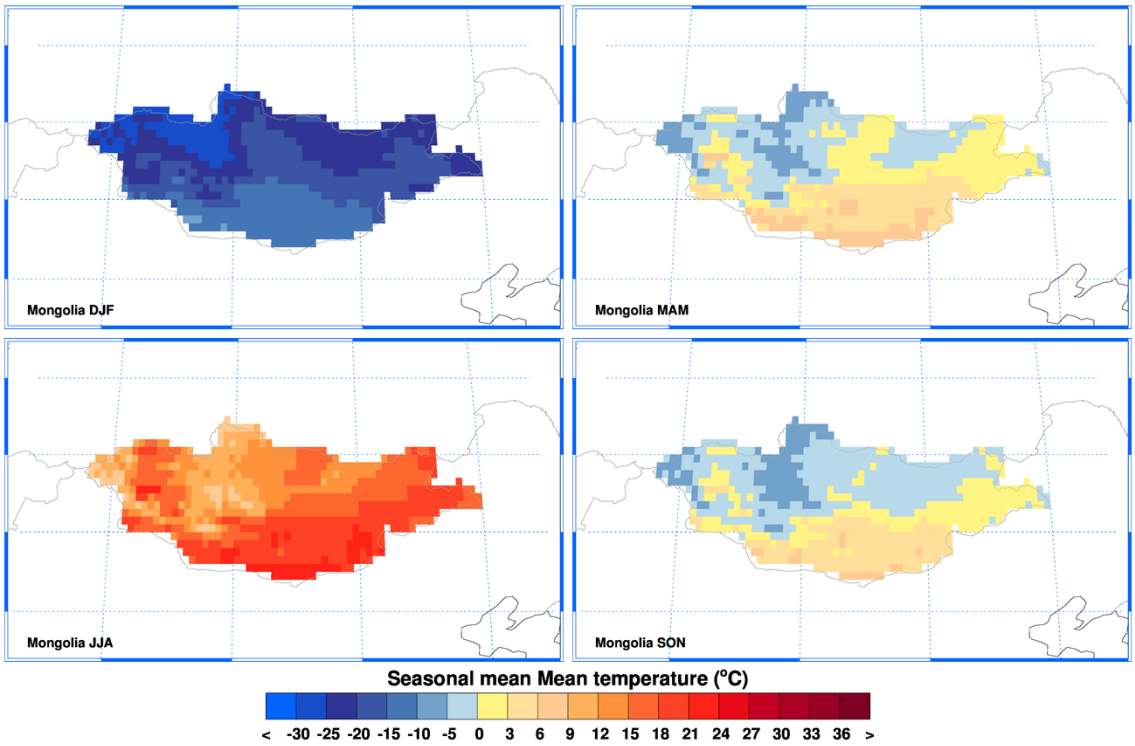


Figure 1-1. Seasonal Mean Temperature in Mongolia

1.3 Scope and Limitations

This thesis focuses on digital engineering for greenhouse design, with all modeling created in Autodesk Inventor. Hardware work is limited to a PID temperature control subsystem, tested on a breadboard within a cardboard enclosure using a 60W heat source. This approach follows a dual methodology: digital design validated by simulation and control logic validated by hardware, with these limitations clearly stated.

The prototype uses a DHT11 temperature sensor (1°C resolution, ±2°C accuracy), which is suboptimal for PID control. A software filter mitigates quantization, and Chapter 6 recommends upgrading to a higher-resolution DHT22.

The validated PID controller only adjusts fan speed. The exhaust louvre remains passive and uncontrollable, while wind direction sensing, humidity, and multi-variable controls are excluded from this study.

2.STATE OF THE ART

2.1. Greenhouse Thermal Environment

Harvesting seasonal produce is challenging in areas with harsh climates [2]. Controlled Environment Agriculture (CEA) addresses this by improving food production despite environmental limits. Accurate temperature control in CEA systems helps maintain crop yields and reduce energy use [3].

Passive solar greenhouses are a popular solution, using solar energy as their main heat source. These greenhouses store heat in walls and soil during the day, releasing it at night, which stabilizes temperatures and supports agriculture without active heating systems [4].

When outdoor temperatures reach 36–39 °C (up to 47 °C at peak), greenhouse interiors can heat up by 8–10 °C, especially with limited ventilation. At solar radiation levels of 500–900 W/m², indoor–outdoor temperature differences of about 8 °C have been observed [5]. Sunlight enters through glazing as short-wave energy, is absorbed, and then re-emitted as long-wave heat, but air's low thermal mass means heat builds up quickly. Glazing further limits heat loss, causing rapid temperature increases under high solar irradiance [6][7].

In Mongolia, where temperatures range from −40 °C in winter to +38 °C in summer, small-scale agriculture faces major greenhouse thermal management challenges. High solar radiation and extreme temperatures can push greenhouse conditions beyond safe plant growth thresholds [2]. Addressing this requires understanding heat exchange and implementing automated control systems to adapt to changing environments.

2.2. Greenhouse Thermal Modeling

The thermal dynamics of a greenhouse follow energy conservation: the change in stored heat equals the net heat gain or loss through its envelope. This is represented by an energy balance equation that underpins the simplified control model and computational fluid dynamics simulation presented in this thesis.

The general form of the greenhouse energy balance is given by:

$$m \cdot C_p \cdot \frac{dT_{in}}{dt} = Q_{solar} - Q_{vent} - Q_{cond}$$

where m is the total mass of air within the greenhouse volume (kg), C_p is the specific heat capacity of air at constant pressure (approximately 1005 J/kg·K), T_{in} is the mean indoor air temperature (°C), and t represents time (s). The three terms on the right-hand side correspond to the three dominant heat transfer mechanisms in a glazed greenhouse: solar radiation heat gain, ventilation-driven heat removal, and conductive heat exchange through the envelope, respectively [8].

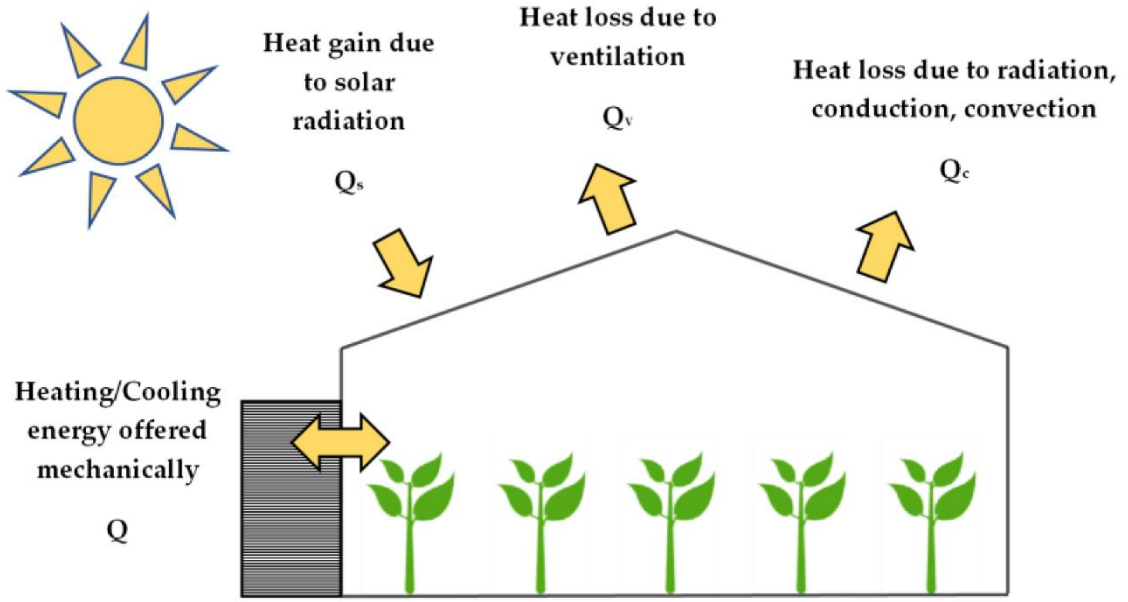


Figure 2-1. Energy Balance in a Typical Greenhouse

Solar radiation constitutes the primary heat input during daylight operation. Incident shortwave solar radiation penetrates the glass covering with a transmittance of approximately 0.85 for standard horticultural glass, is absorbed by the internal surfaces and floor, and is re-emitted as longwave infrared radiation that the glass largely prevents from escaping a mechanism known as the greenhouse effect [9.]. The solar heat gain is quantified as:

$$Q_{solar} = I \cdot A_{glass} \cdot \tau \cdot \alpha$$

where I is the incident solar irradiance (W/m²), A_{glass} is the total transparent envelope area (m²), τ is the glass solar transmittance, and α is the mean absorption coefficient of internal surfaces. For the greenhouse geometry adopted in this thesis, with a total glazed area of approximately 156.48 m² and a peak solar irradiance of 800 W/m² was assumed for clear summer conditions in Ulaanbaatar,

the peak solar heat load is estimated at approximately 70.1 kW, confirming that active thermal management is essential under summer conditions.

Ventilation heat removal represents the primary cooling mechanism and the quantity directly manipulated by the control system. When warm indoor air at temperature $T_{in}$is replaced by cooler outdoor air at T_{out}, the rate of heat extraction is:

$$Q_{vent} = \dot{m}_{air} \cdot C_p \cdot (T_{in} - T_{out})$$

where $\dot{m}_{air}$ is the mass flow rate of ventilation air (kg/s). This expression reveals an important limitation of ventilation-based cooling as the outdoor temperature approaches the indoor temperature, the temperature differential $(T_{in} - T_{out})$ diminishes, reducing the effectiveness of ventilation regardless of the airflow rate achieved [10]. This condition, which arises on extreme summer days, motivates the forced ventilation strategy adopted in the present design.

Conductive heat exchange through the greenhouse envelope follows Fourier's Law of heat conduction, expressed in the form:

$$Q_{cond} = U \cdot A_{envelope} \cdot (T_{in} - T_{out})$$

where U is the overall heat transfer coefficient of the glazing material (W/m²·K) [11]. In summer, this pathway allows interior heat to escape and enhances cooling from ventilation. In colder conditions, it becomes the main route for heat loss, as indoor temperatures exceed outdoor levels and conduction reduces heat retention.

The energy balance model treats the greenhouse as having a uniform temperature, which is useful for overall control but does not address internal variations in temperature and airflow. To overcome this, computational fluid dynamics simulations are used alongside the energy model to capture spatial differences within the greenhouse.

2.3. Ventilation Systems in Greenhouses

Ventilation is the primary active mechanism for maintaining thermal equilibrium inside a greenhouse under conditions of high solar heat gain. Its role is not limited to removing heat from the internal air volume; it also helps maintain spatial temperature uniformity across the greenhouse cross-section and provides the

airflow needed to sustain the temperature difference required for effective heat extraction, as described in Section 2.2. Greenhouse ventilation systems are generally classified as either natural, where airflow is driven passively by buoyancy and wind pressure, or mechanical, where airflow is generated by electrically powered fans [12]. Although natural ventilation has been widely studied and remains common in low-cost greenhouse construction, its dependence on favorable ambient conditions makes it unsuitable as the primary temperature control strategy for the present design. In the continental climate of Ulaanbaatar, Mongolia, where peak summer ambient temperatures can approach 35°C, the indoor–outdoor temperature difference available to drive passive airflow may be insufficient to maintain the target internal temperature on the hottest days [12] This thesis uses mechanical forced ventilation, supported by a perforated duct network that enhances spatial uniformity beyond what a direct fan-to-exhaust setup can provide. The next sections outline the engineering fundamentals and design principles for forced ventilation and perforated duct systems.

2.3.1 Forced Mechanical Ventilation

Forced mechanical ventilation uses electrically driven fans to move air through the greenhouse enclosure, decoupling the ventilation rate from ambient wind speed, wind direction, and the indoor–outdoor temperature differential that governs passive systems. Unlike natural ventilation, forced-air systems provide predictable airflow rates and a defined direction of air movement.[13] This predictability is an important engineering advantage for automated control systems, since stable PID tuning requires a consistent and quantifiable relationship between fan output, airflow rate, and the resulting temperature response [13].

In forced ventilation, a fan moves air from an intake (usually low) to an exhaust (usually high), following the natural rise of warm air. Proper placement of these openings boosts efficiency by supporting buoyancy-driven airflow, which lowers the energy needed to ventilate the greenhouse [12]. This principle informs the intake and exhaust placement in the present design, where the intake fan is positioned on the north wall at 30 cm above floor level and the exhaust opening is located on the south wall at 2 m height.

Forced longitudinal or transverse ventilation inevitably produces a temperature gradient along the airflow direction, because incoming air absorbs heat as it moves through the greenhouse from intake to exhaust [13]. The air near the inlet stays

cooler than at the outlet, creating a temperature gradient across the 6 m greenhouse from north (intake) to south (exhaust). Increasing airflow reduces this gradient, but fan speed alone can't remove it. This persistent unevenness is why the perforated duct system in Section 2.3.2 was added.

2.3.2 Holed Duct Air Distribution Systems

Discharging air from one intake in a long greenhouse often causes uneven airflow and temperature, especially far from the intake. The air jet concentrates along the center, leaving sidewalls and floors with weak mixing, low velocities, and higher temperatures [14]. Holed ducts address this limitation by distributing the fan output through a series of regularly spaced openings along the length of a pipe, allowing conditioned air to enter the greenhouse at multiple points rather than from a single location.

A perforated duct system uses a fan to push air through a polyethylene or PVC tube inside a greenhouse. Air exits via holes along the duct, mixing evenly with internal air [15]. The size, spacing, and angle of the holes affect how uniformly air is delivered and mixed throughout the greenhouse.

Perforated duct design faces the issue of static pressure dropping from inlet to capped end, leading to stronger airflow near the inlet. Under turbulent conditions, a mathematical model determined a discharge coefficient of about 0.65 and found that jet angles change along the duct due to varying velocity and total head [16].To achieve uniform air distribution, designers should adjust hole spacing or diameter to compensate for the pressure gradient [17].

CFD-based optimization studies have identified hole diameter, hole spacing, and inlet velocity as the three main parameters governing perforated duct performance. Larger hole diameters generally improve velocity uniformity along the duct, while wider hole spacing tends to reduce uniformity. Pressure loss shows the opposite trend: configurations that improve uniformity usually require higher fan pressure and therefore greater energy consumption [17]

The perforation discharge angle significantly influences air jet mixing in the greenhouse. In this design, perforations are set at a 45° downward angle to direct airflow toward the plant zone near the floor. Jet outlet velocity determines local air speed, and the overall distribution depends on several interacting factors The 45° downward orientation helps the air reach the lower zone with enough momentum

to promote vertical mixing, reducing thermal stratification that would otherwise leave warm air near the roof and cooler air near the floor [18]. Such stratification would reduce ventilation effectiveness and weaken the representativeness of the temperature signal used by the PID controller.

2.4 CFD Simulation of Greenhouse Environments

Computational fluid dynamics (CFD) is the numerical solution of the governing equations of fluid motion and heat transfer over a discretised geometry. In the greenhouse context, CFD has become the standard methodology for resolving the spatial distribution of temperature and airflow that the lumped-parameter energy balance of Section 2.2 cannot capture. CFD is particularly suited to greenhouse studies because the typical airflow is incompressible, the Mach number is far below 0.3, the geometry is bounded, and the dominant physical phenomena buoyancy-driven convection, forced advection, and mixed boundary heat exchange are all well represented within commercial RANS solvers such as ANSYS Fluent.

2.4.1 Governing Equations

The flow inside a ventilated greenhouse is governed by the steady-state, three-dimensional Reynolds-Averaged Navier-Stokes (RANS) equations together with the energy equation. The continuity equation expresses mass conservation; the three momentum equations express Newton's second law applied to a fluid element; and the energy equation expresses conservation of thermal energy. For incompressible airflow with buoyancy effects, the Boussinesq approximation is applied: the air density is treated as constant in all terms except the gravitational body force, where it is allowed to vary linearly with temperature through the thermal expansion coefficient β. This approximation is valid when the temperature variations within the domain remain below approximately 30 K, a condition satisfied in the present greenhouse [20].

2.4.2 Turbulence Modelling

Direct resolution of all turbulent scales (DNS) is computationally infeasible at greenhouse scale; turbulence is therefore modelled rather than resolved. The two-equation k-ε family is the most widely adopted closure in indoor airflow studies because it offers a favourable balance of accuracy and computational cost. Among its variants, the k-ε realizable model improves the standard k-ε in flows involving

rotation, recirculation, and adverse pressure gradients—all features present in greenhouse flows around obstacles, near outlets, and within recirculation zones generated by buoyancy. Published greenhouse CFD studies consistently report good agreement between k-ε realizable predictions and field measurements for both natural and forced ventilation configurations.

2.4.3 Boundary Conditions and Numerical Approach

Greenhouse CFD models typically employ a velocity-inlet boundary at the intake, a pressure-outlet boundary at the exhaust, mixed (convective + radiative) boundary conditions on the glazed envelope, and a prescribed surface heat flux on the floor representing absorbed solar radiation. The pressure-velocity coupling is generally handled by the SIMPLE algorithm, with second-order upwind discretisation of the convective terms in the momentum, energy, and turbulence equations. Convergence is assessed through residual monitoring, with energy residuals required to fall below 1×10^{-6} due to the small temperature gradients involved, and momentum and turbulence residuals required to fall below 1×10^{-4}.

2.4.4 Application to Forced Ventilation Greenhouses

Several published CFD studies have specifically addressed forced ventilation greenhouses. Li et al. evaluated airflow patterns and thermal behaviour of arched greenhouses with various roof ventilation scenarios, demonstrating that CFD can resolve gradients of 3–6 K across the greenhouse cross-section that simple energy balance models could not predict. Benni et al. used CFD coupled with environmental monitoring to validate natural ventilation effectiveness in a Mediterranean greenhouse, while Liu et al. applied CFD specifically to optimise temperature sensor placement in a pad-fan cooled greenhouse, finding that sensor location strongly affects the representativeness of the measured signal—an outcome directly relevant to the sensor placement decision in Section 3.7. Tadj et al. applied CFD to perforated polyethylene heating ducts and demonstrated that hole-spacing tapering can be analytically designed to compensate for static pressure decay, producing approximately uniform jet velocity along the duct length. These studies collectively support the methodological choices adopted in Chapter 4 and Chapter 5 of this thesis.

2.5. Control Systems for Greenhouse Temperature

2.5.1 The Greenhouse as a Control Problem

The greenhouse thermal environment can be modeled as a dynamic system subject to continuous external disturbances, including solar irradiance, ambient temperature, and wind. These inputs cannot be controlled directly and must instead be compensated through active regulation. As a result, effective temperature control requires a feedback system that continuously measures the indoor temperature, compares it to a desired setpoint, and applies corrective action based on the deviation [19].

Open-loop strategies, such as operating a fan at constant speed, are insufficient because they cannot adapt to time-varying disturbances. For this reason, feedback control of greenhouse ventilation has been widely studied, with the proportional–integral–derivative (PID) controller emerging as the most used approach in both research and practical applications [20].

2.5.2 Feedback Control Fundamentals

A feedback control loop consists of four main components operating continuously. A sensor measures the controlled variable, which in this work is the indoor air temperature obtained from a DHT11 sensor. The controller computes a corrective signal based on the difference between the measured value and the setpoint. The actuator converts this signal into a physical action, in this case fan speed controlled via PWM through a MOSFET. The resulting change in temperature is then fed back to the sensor, closing the loop [19].

The error signal is defined as:

$$e(t) = T_{set} - T_{in}(t)$$

When $e(t) < 0$, the indoor temperature exceeds the setpoint and cooling must be increased. When $e(t) > 0$, the temperature is below the setpoint, and no additional cooling is required. The objective of the controller is to drive this error toward zero and maintain it despite ongoing disturbances.

2.5.3 The PID Controller

A PID controller generates its output as the sum of three components, each responding to a different aspect of the error signal: present, accumulated, and predicted behavior. This structure has remained dominant in industrial control due to its simplicity, robustness, and broad applicability [21].

The control law is given by:

$$u(t) = K_p e(t) + K_i \int_0^t e(\tau)\, d\tau + K_d \frac{de(t)}{dt}$$

where $u(t)$ is the controller output (mapped to fan PWM duty cycle), and K_p, K_i, and K_d are the proportional, integral, and derivative gains.

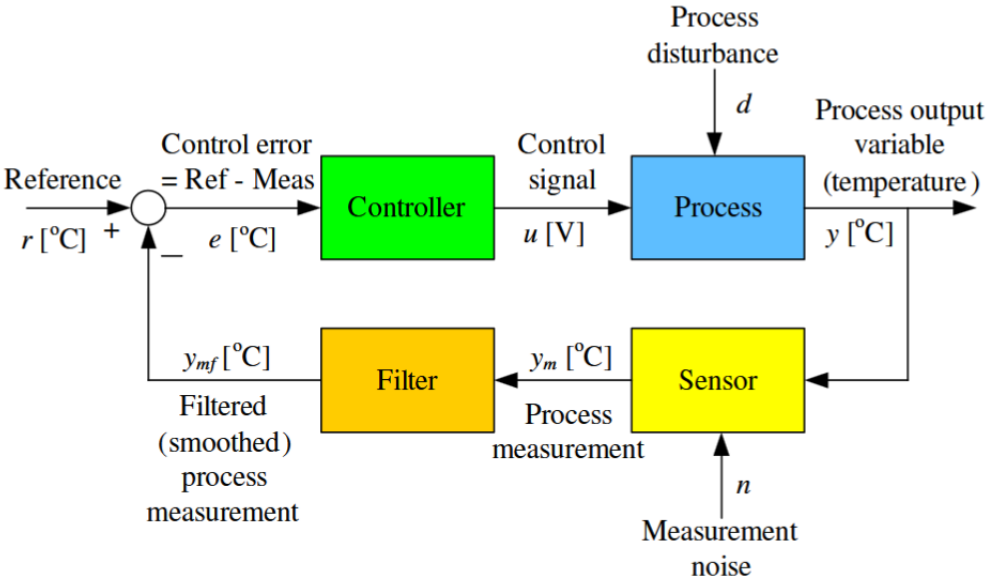


Figure 2-2. Block Diagram of the Temperature Control System

2.5.4 Proportional Term

The proportional term produces an output directly proportional to the current error. Large deviations from the setpoint result in strong corrective action, while smaller errors produce weaker responses. This enables smooth, continuous control compared to ON/OFF switching [21]. However, proportional control alone cannot eliminate steady-state error, as zero error would imply zero control action, which is insufficient to balance a persistent heat load.

2.5.5 Integral Term

The integral term accumulates the error over time and increases the control output when a sustained offset exists. This allows the controller to eliminate steady-state error by compensating for persistent disturbances such as continuous solar heat gain [21].

A practical issue is integral windup, which occurs when the actuator saturates and the integral term continues to grow. This can lead to overshoot once the system recovers. In this implementation, anti-windup is handled by limiting the integral term when the PWM output reaches its bounds.

2.5.6 Derivative Term

The derivative term $K_d \frac{de(t)}{dt}$ responds to the rate of change of error. It acts as a damping mechanism by reducing the control action when the system approaches the setpoint rapidly, thereby limiting overshoot [21]. It also improves responsiveness to sudden disturbances.

However, derivative action is sensitive to measurement noise. Given the characteristics of the DHT11 sensor, derivative noise is managed by applying a low-pass filter to the error derivative before it enters the control calculation [22].

2.5.7 PID Tuning Ziegler Nichols Method

The controller gains K_p, K_i, and $K_d$are determined using the Ziegler–Nichols closed-loop tuning method, which is suitable when an analytical model of the system is not available [23].

The procedure is as follows:

1. Set $K_i = 0$and $K_d = 0$, leaving only proportional control.
2. Increase $K_p$until the system exhibits sustained oscillations. Record this gain as the ultimate gain $K_u$and the oscillation period as T_u.
3. Compute the PID gains using:

$$K_p = 0.6K_u, K_i = \frac{2K_p}{T_u}, K_d = \frac{K_p T_u}{8}$$

These values serve as initial estimates. Further manual adjustment is typically required to reduce overshoot, since the standard Ziegler–Nichols tuning often produces an aggressive response with approximately 25% overshoot, which may be unsuitable for temperature-sensitive applications [23].

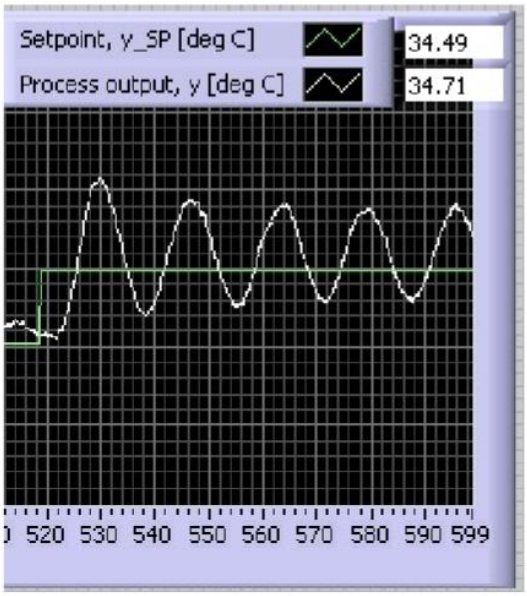


Figure 2-3. Ziegler-Nichols Ultimate Gain method; Response with ultimate gain

2.5.8 Digital Implementation on Arduino

The continuous PID equation is discretized for implementation on the Arduino Uno, which operates at fixed sampling intervals. The integral term is approximated as a cumulative sum, and the derivative term is computed using a backward difference:

$$u[n] = K_p \cdot e[n] + K_i \cdot T_s \sum_{k=0}^{n} e[k] + K_d \cdot \frac{e[n] - e[n-1]}{T_s}$$

where T_s is the sampling period and n is the discrete time index. The Arduino Uno microcontroller is well suited to PID temperature control applications, providing sufficient processing capability to execute the PID algorithm, read sensor data, update the display, and generate the PWM output signal within a single sampling interval [24]. The computed output $u[n]$ is mapped to an 8-bit PWM value between 0 and 255, which is applied to the MOSFET gate to modulate the fan speed proportionally. The relay module provides an independent safety layer, triggering

an emergency fan shutdown if the temperature exceeds a configurable upper safety limit regardless of the PID output state.

2.6 Research Gap and Thesis Positioning

2.6.1 Summary of Established Knowledge

The preceding review demonstrates that greenhouse thermal management and ventilation control are well studied topics with a substantial published foundation. The governing energy balance for greenhouse heat transfer is well established, and the thermal advantages of twin-wall polycarbonate over single-layer glazing are documented [25]. Perforated duct air distribution systems have been analytically modelled and validated, with multiple studies confirming improved spatial uniformity compared to direct fan to exhaust configurations [26], [27]. PID control remains the dominant strategy for automated greenhouse temperature regulation, and the Ziegler-Nichols method provides a reliable approach for gain tuning when an explicit plant model is unavailable [28], [29]. Low-cost embedded implementations using Arduino-class microcontrollers have demonstrated the practical feasibility of PID temperature control without industrial instrumentation [30].

2.6.2 Identified Gaps in the Literature

Despite this scale of knowledge, three specific gaps relevant to the present thesis are identified.

The first gap concerns the engineering justification of low-cost hardware implementations. Published Arduino-based greenhouse controllers typically select sensor placement, fan sizing, and duct configuration based on convenience or empirical judgment rather than systematic engineering analysis [30]. This absence of traceable justification limits the reproducibility and transferability of such designs. A low-cost hardware implementation whose physical design parameters are explicitly derived from peer-reviewed literature duct perforation ratios, sensor height, fan face velocity represents a contribution that bridges the gap between academic rigor and practical affordability.

The second gap concerns climate specificity. The overwhelming majority of published greenhouse control and ventilation studies target Mediterranean, temperate European, or humid subtropical climates [31], [32]. The continental semi-arid climate of Ulaanbaatar, Mongolia characterized by peak summer temperatures of 35°C, peak solar irradiance exceeding 800 W/m², and winter temperatures as low as -30°C imposes a thermally extreme design environment that is essentially absent from the published literature. Existing design guidelines developed for mild temperate climates cannot be directly applied to the Mongolian context without climate-specific adaptation.

The third gap concerns the integration of analytical duct design with hardware control validation. Studies on perforated duct systems primarily address fluid mechanical performance in isolation [26], [27], while Arduino PID studies address control logic without reference to the physical ventilation design [30]. No study identified in this review presents a unified engineering framework in which the ventilation duct system is analytically designed and justified using published hydraulic models, and a PID controller is physically implemented and experimentally validated on the same system at laboratory scale.

2.6.3 Thesis Positioning

The present thesis addresses all three identified gaps within a single integrated study.

In response to the first gap, every physical design decision in this thesis is explicitly traceable to a peer-reviewed source. The progressive hole spacing strategy follows the pressure-compensation approach validated by Tadj et al. [27]. The fan face velocity of 4.0 m/s follows standard greenhouse ventilation engineering guidance [33]. The sensor placement at 1.2m height is consistent with CFD-based sensor optimisation studies [34]. This traceability distinguishes the present design from the empirical low-cost implementations documented in the literature.

In response to the second gap, all design parameters, thermal load calculations, and boundary conditions are defined specifically for the climate of Ulaanbaatar, Mongolia (47.9°N latitude). The peak solar irradiance of 800 W/m², ambient design temperature of 35°C, and North-wall intake placement are all climate-responsive decisions embedded in the design, positioning the present work as one of the first

documented engineering studies of a PID-controlled forced ventilation greenhouse explicitly adapted for the Mongolian continental climate.

In response to the third gap, this thesis presents an integrated framework in which the three-branch perforated PVC duct system is analytically characterised using the Teitel hydraulic model and compared against published duct performance benchmarks, while the PID temperature controller is implemented on Arduino Uno hardware and experimentally validated in simulation. The convergence between analytically predicted duct performance and experimentally measured controller response constitutes the dual-validation contribution of the thesis.

2.6.4 Thesis Objectives

Objective 1: To design a single-span forced ventilation greenhouse structurally adapted to the continental semi-arid climate of Ulaanbaatar, Mongolia, with all geometric parameters, glazing material properties, and peak thermal load calculations explicitly derived from peer-reviewed sources, and the complete geometry realized as a parametric 3D model in Autodesk Inventor.

Objective 2: To design a three-branch perforated PVC duct air distribution system in which perforation spacing is tapered following the Teitel hydraulic pressure-compensation model, with all duct geometry parameters branch diameter, hole diameter, hole count, discharge angle, and spacing progression justified against published duct performance guidelines.

Objective 3: To implement a discrete-time PID temperature controller on Arduino Uno, with fan speed modulated via PWM through a MOSFET, relay-based secondary actuation at 50% output threshold, anti-windup clamping, and an independent safety cutoff at 45°C, with all gains derived from the Ziegler–Nichols closed-loop method.

Objective 4: To verify the algorithmic correctness of the PID controller through four structured simulation scenarios in Wokwi step response, setpoint tracking, disturbance rejection, and anti-windup operation confirming that all twelve specified control behaviors are exhibited, and to identify the quantitative performance characterization that physical hardware testing must subsequently provide.

3. SYSTEM DESIGN

3.1 Chapter Overview

This chapter presents the complete engineering design of the smart greenhouse forced ventilation system developed in this thesis. The design includes three integrated subsystems: the greenhouse physical structure, the forced ventilation and air distribution network, and the PID based temperature control hardware.

3.2 Greenhouse Context and Orientation

3.2.1 Site Context and Orientation

The continental semi-arid climate enforces a demanding thermal design brief: peak summer ambient temperatures of approximately 35°C combined with peak solar irradiance exceeding 800 W/m² create severe overheating risk, while winter temperatures as low as -30°C demand effective heat retention from the same envelope [35]. The greenhouse is oriented with its long axis running East-West, a standard configuration for Northern Hemisphere installations that maximizes uniform solar exposure across the full width of the growing area throughout the day [36].

The intake fan is positioned on the North wall. This placement is a deliberate climate responsive decision: in the Northern Hemisphere, the North-facing wall receives minimal direct solar radiation and therefore presents the coolest available air on the external face of the building. Introducing ventilation air from the coolest external face maximizes the temperature differential available for heat extraction, consistent with the $Q_{vent} = \dot{m}_{air} \cdot C_p \cdot (T_{in} - T_{out})$ relationship established in Section 2.2.

The greenhouse structural design presented in this chapter constitutes a complete digital engineering design, realised as a parametric 3D model in Autodesk Inventor. No physical greenhouse structure is constructed within the scope of this thesis. The hardware contribution is limited to the PID temperature control subsystem, which is validated in a laboratory thermal test environment as described in Section 3.6.

3.2.2 Geometric Parameters

Table 3.1: Greenhouse Geometric Parameters

PARAMETER	VALUE	BASIS
Length (East-West)	10m	Literature-consistent single-span
Width (North–South)	6m	Standard single-span width [2]
Sidewall Height	2.6m	Practical working clearance
Ridge Height	3.68m	~20° roof slope
Roof Slope Angle	20°	Calculated from width and heights
Internal Volume (V)	~189 m^3	Calculated (Section 3.3)
Total Glazed Area (A)	~153 m^2	Calculated (Section 3.3)

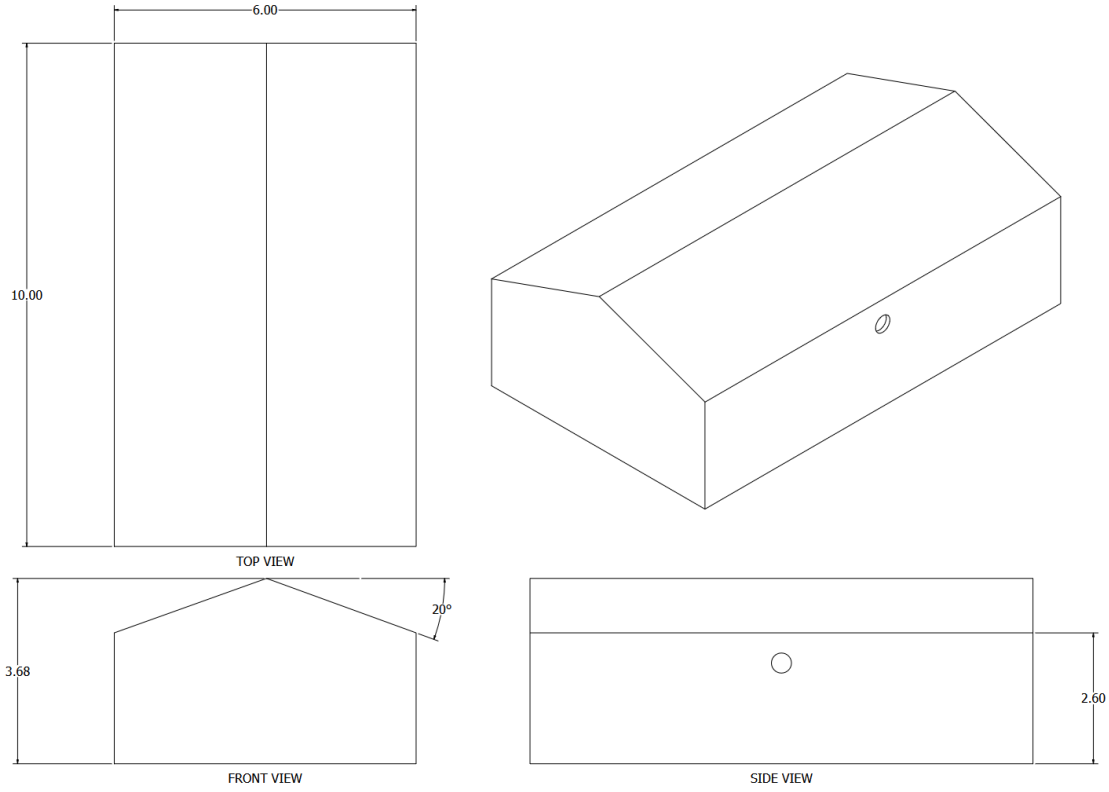


Figure 3-1. Isometric View of Greenhouse Design

The roof slope of 20° is a considered engineering decision. A steeper slope increases the ridge height and internal volume, which benefits natural buoyancy-assisted airflow but increases the glazed area and therefore the solar heat load. A shallower slope reduces heat load but compromises the vertical separation between intake and exhaust that assists thermally stratified airflow. The 20° angle

represents a practical compromise validated by the 3.6m ridge height, which provides 1.3m of vertical separation between the intake at 0.3m and the exhaust at 2.0m sufficient to produce measurable buoyancy assistance to the forced airflow.

3.2.3 Glazing Material

The greenhouse is clad entirely in 16mm twin-wall polycarbonate panels. The selection of this material over single-layer glass is justified by three engineering advantages relevant to the Mongolian climate context. First, the twin-wall cellular structure reduces the overall heat transfer coefficient to approximately 3.2 W/m²·K, compared with 5.8–6.2 W/m²·K for single-layer glass a 45% improvement in thermal insulation that directly reduces heat loss during cold winter nights and lowers the heating energy requirement [38]. Second, the solar transmittance of 0.73 reduces peak solar heat gain relative to glass, lowering the peak cooling load from approximately 79 kW (glass equivalent) to 58.2 kW. Third, polycarbonate panels are significantly lighter and more impact-resistant than glass, reducing the structural load on the steel frame and improving resistance to hail a relevant consideration for the Mongolian steppe environment.

The thermal and optical properties of the glazing material used throughout this thesis are summarized in Table 3.2.

Table 3.2: Polycarbonate Glazing Thermal and Optical Properties

PROPERTY	VALUE	SOURCE
Thickness	16 mm twin-wall	Specified
Overall U-Value	3.2 W/m²·K	Manufacturer / [4]
Solar Transmittance (T)	0.73	Manufacturer / [4]
Infrared Emissivity	0.90	Standard glazing [4]
Solar Absorptance (Internal Surfaces)	0.65	Standard assumption [1]

3.3 Thermal Load Analysis

3.3.1 Internal Volume and Glazed Area Calculation

The internal air volume is calculated as the product of the floor area and the mean internal height, where the mean height approximates the trapezoidal cross-section of the gable roof:

$$\bar{h} = h_{wall} + \frac{1}{2}\left(h_{ridge} - h_{wall}\right) = 2.6 + \frac{1}{2}(3.68 - 2.6) = 3.14 \text{ m}$$

$$V = L \times W \times \bar{h} = 10 \times 6 \times 3.14 = 188.4m^3$$

The total glazed area is calculated by summing all envelope surfaces. Two long sidewalls contribute $2 \times (10 \times 2.6) = 52\text{m}^2$. Two roof slopes, each with a developed length of $\sqrt{3^2 + 1.08^2} \approx 3.19m.$ and a length of 10m, contribute $2 \times (3.19 \times 10) = 63.8m^2$ Two gable end walls, each comprising a rectangular lower section of $(6 \times 2.6) = 15.6\text{m}^2$ and a triangular upper section of $\frac{1}{2} \times 6 \times 1.08 = 3.24\text{m}^2$, contribute $2 \times 18.84 = 37.68$. The total glazed area is therefore:

$$A_{glaz} = 52 + 63.8 + 37.68 = 155.6m^2$$

3.3.2 Peak Solar Heat Gain

Applying the solar heat gain equation from Section 2.2 with the confirmed polycarbonate properties and Ulaanbaatar peak summer irradiance:

$$Q_{solar} = I \cdot A_{glaz} \cdot \tau \cdot \alpha = 800 \times 153.6 \times 0.73 \times 0.65 = 58.3 \text{ kW}$$

This value is the peak thermal load used to size the ventilation system and serves as the basis for all ventilation and fan calculations.

3.3.3 Required Ventilation Rate

The required volumetric airflow rate to maintain the indoor temperature at the design setpoint of 25°C against the peak solar heat gain is derived from the ventilation heat removal equation of Section 2.2, rearranged for $\dot{Q}$:

$$\dot{Q} = \frac{Q_{solar}}{\rho \cdot C_p \cdot (T_{in} - T_{out})} = \frac{58200}{1.10 \times 1005 \times (35 - 25)} = 5.26m^3/s = 18{,}936m^3/h$$

This result is checked against the air changes per hour metric. The required ACH is:

$$ACH = \frac{\dot{Q}}{V} = \frac{5.26}{188.4/3600} \approx 100.5 \text{ ACH}$$

This is a high value reflecting the severity of the peak thermal load under Mongolian summer conditions. In practice, the fan is not expected to maintain 25°C setpoint under peak irradiance with only 10°C outdoor-indoor differential a physical constraint acknowledged as a design limitation in Chapter 6. The design target of 30 ACH is therefore adopted as a practical operating target, corresponding to a fan airflow of:

$$\dot{Q}_{design} = \frac{30 \times 188.4}{3600} = 1.57 m^3/s = 5{,}652 m^3/h$$

3.4 Ventilation System Design

3.4.1 Fan Placement and Airflow Path

The ventilation system pushes air from a North wall intake fan across the 6m width of the greenhouse to a fixed exhaust on the South wall. This transverse setup was chosen instead of a longitudinal one because the shorter path reduces fan pressure needs and temperature gradients, and it leverages thermal stratification: cool air enters low, warms up as it moves through, rises, and exits high, lowering energy use. The South wall exhaust is a fixed louvre sized to keep air velocity under 2.0 m/s, preventing bottlenecks. The exhaust area required is:

$$A_{exhaust} = \frac{\dot{Q}_{design}}{v_{exhaust}} = \frac{1.57}{2.0} = 0.79 m^2$$

An exhaust opening of $0.4m$ diameter $0.502\ m^2$ is therefore specified, positioned on the South wall centred at 2.0m height.

3.5 Perforated Duct Air Distribution System

3.5.1 Design Reasoning

Direct single-point discharge from the intake fan would concentrate the incoming airflow along the North wall, creating a pronounced temperature gradient from North to South and leaving the plant zones near the South wall poorly ventilated. The three-branch perforated PVC duct system distributes the fan output at multiple points across the 10m greenhouse length, addressing this non-uniformity as established by the literature reviewed in Section 2.3.2.

3.5.2 Duct Layout and Dimensions

The duct network comprises a main header duct running along the interior of the North wall, connected to three branch ducts running East-West across the full 5.4m width. The branch ducts are spaced at 1.9m, 5.0m, and 7.9m from the North wall dividing the 10m length into three zones of influence. The distal ends of all branches are capped, ensuring all fan-delivered air exits exclusively through the holes. The duct geometry parameters are summarized in Table 3.3.

Table 3.3: Perforated Duct System Parameters

PARAMETER	VALUE	BASIS
Branch Pipe Material	117mm PVC	Standard agricultural ducting
Branch Pipe Internal Diameter	110mm	Standard 110mm PVC specification
Branch Pipe Length	5m	
Number Of Branches	3	Equal zone coverage
Branch Spacing Along Length	3m	10m division
Perforation Diameter	12mm	Literature guidance [5]
Perforation Spacing	300, 250, 200mm	Literature guidance [5]
Perforation Angle	45° downward	Floor-zone targeting
Number Of Holes Per Branch	40	
Total Perforation Area Per Branch	4500 mm²	40 × π(6mm)²
Pipe Cross-Section Area	9005 mm²	π(55mm)²
Far End Condition	Capped	All air through perforations

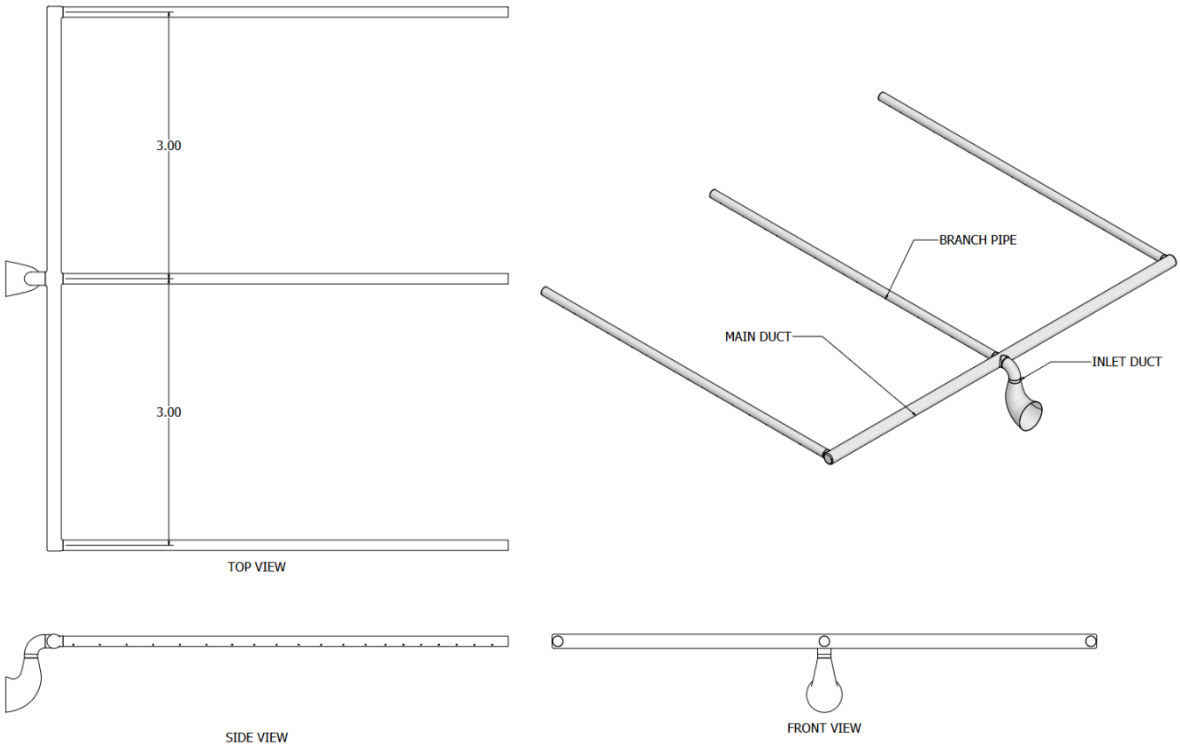


Figure 3-2. Isometric View of Duct System

3.5.3 Perforation Spacing Tapering

As established in Section 2.3.2, static pressure decreases along the duct length from inlet to capped end, causing non-uniform discharge if perforations are evenly spaced. To compensate, the perforation spacing is tapered wider near the inlet and closer near the capped end following the analytical model of Teitel et al. [38]. The inlet-end spacing is set at 300mm for the first third of each branch, reducing to 250mm in the middle third and 200mm in the final third nearest the capped end. This progressive reduction in spacing compensates for the falling internal pressure, promoting approximately uniform jet velocity across the full branch length.

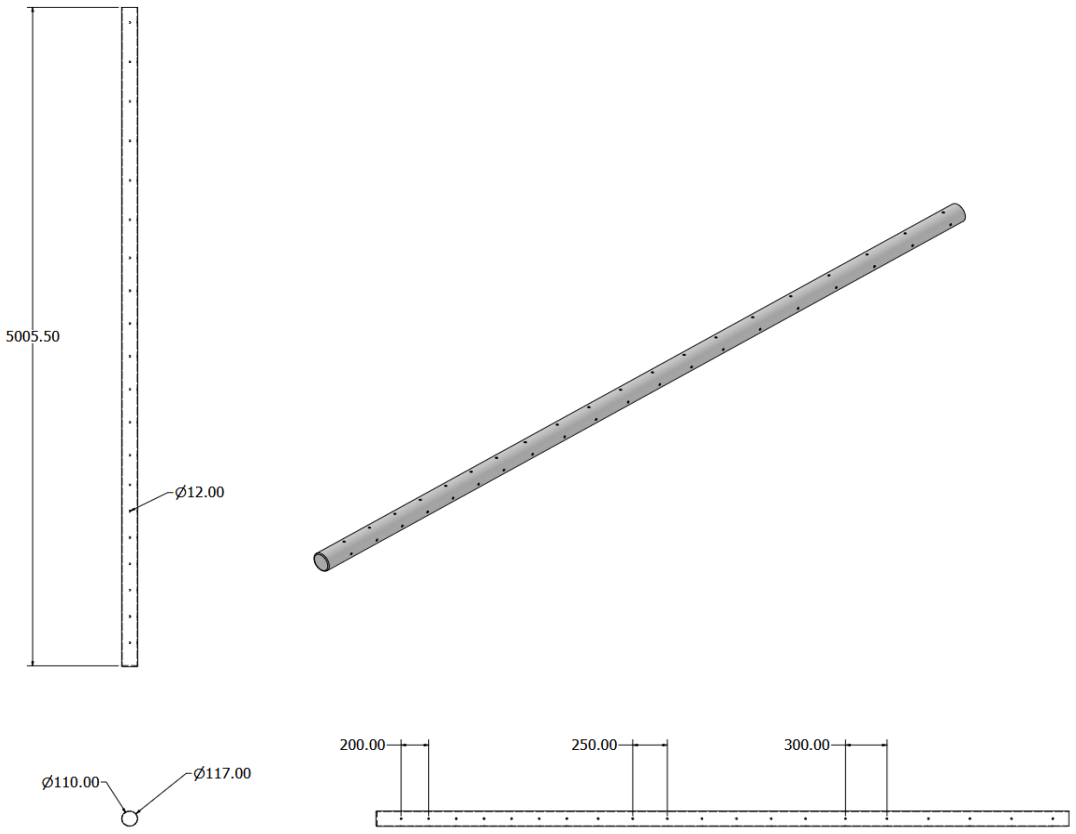


Figure 3-3. Isometric View of Branch Duct

3.5.4 Discharge Angle

The perforations are drilled at 45° downward from horizontal on the underside of the pipe. This angle directs discharged air jets toward the floor-level plant zone, promoting vertical mixing and counteracting the thermal stratification that naturally accumulates warm air near the roof. A purely horizontal discharge would produce jets that traverse the greenhouse cross-section without penetrating the near-floor zone effectively, leaving the lower working area poorly mixed.

The complete greenhouse design can be found in Appendix A.

3.6 Control System Design

3.6.1 System Overview

The control system uses a discrete-time PID algorithm on an Arduino Uno to regulate temperature via PWM. The hardware prototype tests only the PID subsystem, and the greenhouse structure is modeled digitally. There is no physical greenhouse or fan in the prototype. A relay module controls a 60W bulb as a heat source, while a yellow LED managed by a MOSFET visually represents the fan speed based on PID PWM output. This setup enables complete validation of the PID logic sensor input, error calculation, gain adjustment, output control, and safety features in a lab setting. Table summarizes the main components and their functions in both the prototype and proposed system.

Table 3.4: Control System Hardware Components

COMPONENT	MODEL	PROTOTYPE ROLE	FULL-SCALE ROLE
Microcontroller	Arduino Uno (ATmega328P)	PID computation, PWM, display, I/O	
Temperature/ Humidity Sensor	DHT11	Reads box temperature every 1s	Reads greenhouse T_{in}
Power MOSFET	IRFZ44N	Drives yellow LED (fan substitute)	PWM fan speed modulation
Flyback Diode	1N4007	Circuit protection	Inductive load protection

Relay Module	5V single channel	Controls heat bulb (cooling substitute)	Emergency safety cutoff
TFT Display	SPI color TFT	Shows T_{in}, T_{set}, PID output %	
Push Buttons	Tactile, 10kΩ pull-down	Setpoint increment / decrement	
Capacitor	100µF 16V electrolytic	Power supply noise filtering	
Resistors	220Ω, 10kΩ	LED limiting, pull-downs, gate	
Yellow Led	5mm	Fan speed indicator (PWM brightness)	Not present replaced by real fan
Blue Led	5mm	System active indicator	
Red Led	5mm	Overheat alarm	

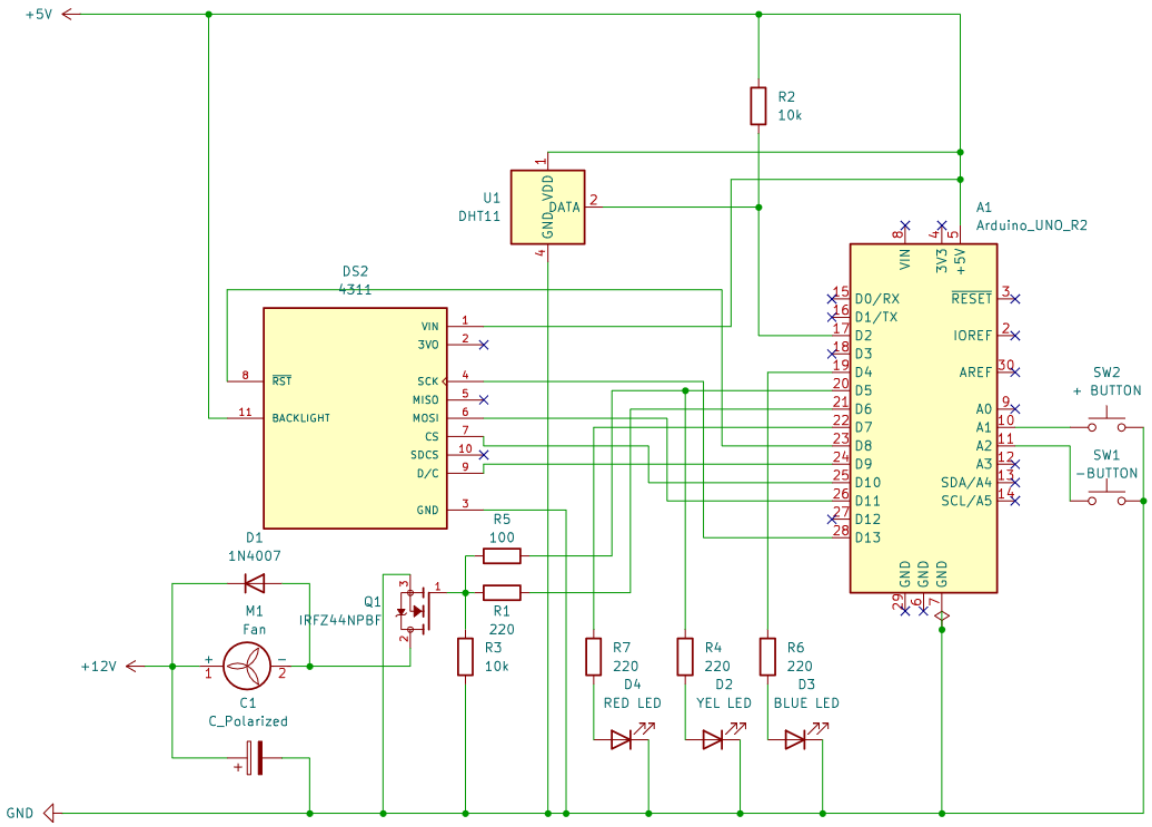


Figure 3-4. The KiCad schematic figure

3.6.2 Signal Flow

The DHT11 sensor reads the temperature of the test enclosure at a fixed sampling interval of $T_s = 1$ second. The Arduino computes the error $e[n] = T_{set} - T_{in}[n]$ and evaluates the discrete PID equation:

$$u[n] = K_p e[n] + K_i T_s \sum_{k=0}^{n} e[k] + K_d \frac{e[n] - e[n-1]}{T_s}$$

The output $u[n]$ is clamped to [0, 255] and written simultaneously to two output channels. The first channel drives the MOSFET gate, modulating the yellow LED brightness as a proportional visual indicator of fan speed command. The second channel drives the relay through a threshold comparison: when $u[n]$ falls below 128 (50% output), the relay opens and disconnects the light bulb, allowing the enclosure to cool; when $u[n]$exceeds 128, the relay closes and the bulb heats the enclosure. This relay threshold implements a hybrid PID-relay actuation scheme in which the continuous PID output governs the LED indicator while the relay provides the binary thermal actuation available in the prototype hardware. The safety cutoff operates independently: if T_{in} exceeds 40°C at any point, the relay opens unconditionally regardless of PID state.

3.6.3 Anti-Windup Implementation

Anti-windup is implemented by clamping the integral accumulator when the computed output $u[n]$reaches its hardware limits of 0 and 255. This prevents the integral term from accumulating beyond the range the actuator can deliver, avoiding the severe overshoot that would otherwise result when the relay switches and the thermal load changes rapidly [39]. For the DHT11 sensor with 1°C resolution, an additional software measure is applied: the derivative term is computed only when the error changes between consecutive samples, and a simple moving average of three consecutive readings is applied before differentiation. This reduces the derivative spikes caused by the sensor's 1°C quantization steps, which would otherwise produce large impulsive outputs at each reading transition [40].

3.6.4 User Interface

Two push buttons allow the user to adjust the temperature setpoint in 1°C increments and decrements, with the current setpoint bounded between 15°C and 35°C. The TFT display continuously shows the current measured temperature, the active setpoint, the PID output as a percentage of maximum, and the system operating mode. The yellow LED brightness varies with PWM output, providing a visible analogue indicator of fan speed in the absence of a physical fan in the prototype. The red LED activates when the relay safety threshold is exceeded.

3.6.5 Sensor Specification and Limitation

The DHT11 temperature and humidity sensor provides a temperature measurement range of 0–50°C with a stated accuracy of ±2°C and a resolution of 1°C. The 1°C resolution means the sensor output advances in discrete integer steps it reports 24°C or 25°C but not 24.3°C. This quantisation introduces a known limitation in the derivative term of the PID controller, since $\frac{de[n]-e[n-1]}{T_S}$ is zero for most samples and spikes to ±1°C/s at each integer transition. The moving average filter described in Section 3.6.3 mitigates this effect. The DHT11 is employed in the prototype as a cost-representative sensor consistent with the low-cost implementation objective of this thesis. Upgrading to a DHT22 sensor which provides 0.1°C resolution and ±0.5°C accuracy is identified as a recommended improvement in Chapter 6, and would produce noticeably smoother PID response curves without requiring any change to the control algorithm or circuit topology [40]. the Wokwi simulation uses DHT22 consistent with this recommendation.

3.7 Temperature Sensor Placement

Sensor placement in a forced ventilation greenhouse is critical. Placing the sensor near the intake or exhaust fans causes inaccurate temperature readings, leading the PID controller to regulate incorrectly. To avoid this, the sensor is placed at the geometric center of the greenhouse plan, 5.0m from the North wall and 3.0m from each sidewall, at a height of 1.2m above the floor the top of the typical plant cover. This position minimizes influence from both intake and exhaust air, yielding an accurate measurement of mean thermal conditions.

4. MATERIALS AND METHODS

4.1 Chapter Overview

This chapter outlines the full implementation and testing methods used to validate the greenhouse design and control system from Chapter 3. Two parallel approaches were applied: a 3D digital model was built in Autodesk Inventor, while the PID temperature controller was tested on the Wokwi. Integrating and cross validating these methods provided the experimental basis for this thesis, with procedures described clearly for reproducibility.

4.2 Greenhouse 3D Model Development

4.2.1 Geometry Construction in Autodesk Inventor

The greenhouse geometry specified in Chapter 3 (Tables 3.1 and 3.2) was modelled in Autodesk Inventor Professional 2026. The model was constructed as a closed hollow shell using a sequential extrusion approach. The floor profile was sketched first as a 10m × 6m rectangle and extruded to the 2.6m sidewall height. The gable roof was added by sketching the triangular cross-section from the sidewall top to the ridge and extruding it along the 10m building length. The result is a watertight solid shell representing the complete greenhouse envelope with no interior obstructions.

4.2.2 Ventilation Openings

Each opening was created using the Extrude Cut tool applied to the relevant wall face, producing clean circular holes with sharp edges. No vent or grille geometry was included, as these features would require excessive mesh refinement to resolve and do not significantly affect the internal flow field.

4.2.3 Perforated Duct Network

The three-branch perforated duct network was modelled according to the parameters in Table 3.3. The main header duct and 3 branch ducts were constructed as cylindrical solid bodies using the Extrude tool, then combined with the greenhouse shell using the Join command to form a single sealed assembly.

4.3 Control System Implementation and Simulation

4.3.1 Simulation Environment

The PID temperature control system was implemented and validated using Wokwi, a browser-based embedded systems simulator that provides cycle-accurate emulation of the Arduino Uno (ATmega328P) microcontroller and associated hardware peripherals, including the DHT22 temperature sensor, PWM output channels, relay module, and LED indicators. Wokwi was selected as the validation environment because it enables complete verification of code execution, signal flow, and component interaction without requiring physical hardware assembly, which falls outside the scope of the present thesis.

It is important to state clearly what Wokwi simulation does and does not validate. The simulator executes the Arduino firmware accurately and reflects correct electrical behavior of the circuit. However, it does not model real thermal dynamics: the DHT22 sensor in Wokwi reads a user-controlled temperature input rather than a physically computed enclosure response governed by thermal mass, heat source inertia, or sensor lag. Consequently, the Wokwi simulation validates the correctness of the PID control algorithm, anti-windup implementation, derivative filter behavior, relay switching logic, safety cutoff, and user interface but it does not substitute for experimental hardware testing with a live thermal load. This distinction between algorithmic validation and thermal performance validation is maintained throughout this chapter and acknowledged as a scope limitation in Chapter 6.

4.3.2 Simulated Circuit Configuration

The circuit was constructed in Wokwi using the following components, consistent with the design specifications of Section 3.6.1:

- Arduino Uno (ATmega328P)
- DHT22 temperature and humidity sensor on digital pin D2
- Yellow LED with 220Ω series resistor on PWM pin D6, representing fan speed
- Red LED with 220Ω resistor on D7, overheat alarm indicator
- Blue LED with 220Ω resistor on D8, system active indicator
- Single channel 5V relay module on D5, representing the backup safety relay

- Two push buttons with 10kΩ pull-up resistors on D3 and D4 for setpoint adjustment.

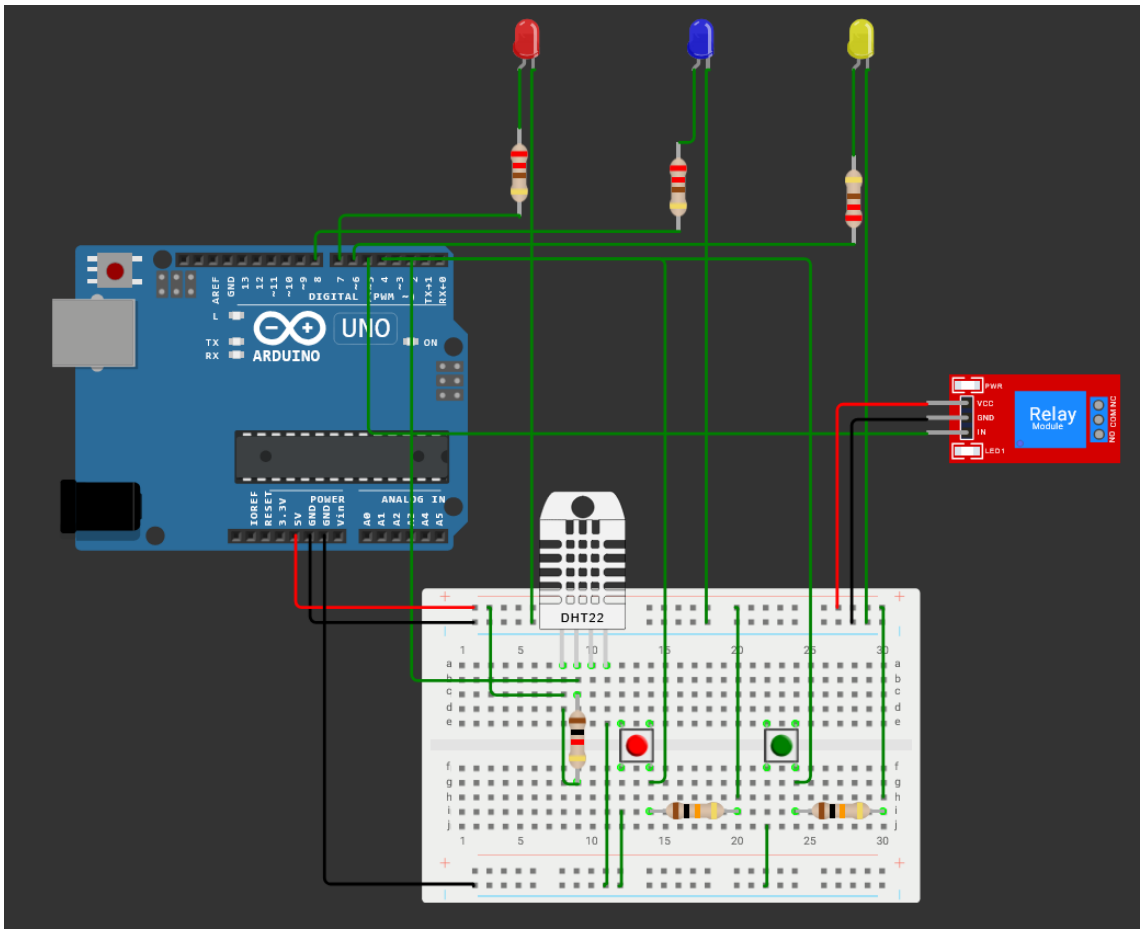


Figure 4-1. The 3D Circuit Visualization generated by Wokwi

Note on sensor substitution: The physical prototype specification in Section 3.6.1 refers to a DHT11 sensor. In the Wokwi simulation, a DHT22 was used, as this is the sensor available in the Wokwi component library. The DHT22 provides 0.1°C resolution and ±0.5°C accuracy, which is the upgraded specification already recommended in Section 3.6.5. No change to the control algorithm or circuit topology is required by this substitution.

4.3.3 Cooling System Control Action

The control system implements a cooling response, consistent with the thermal function of the full-scale greenhouse ventilation system. The error signal is defined as:

$$e[n] = T_{in}[n] - T_{set}[n]$$

When the measured indoor temperature T_{in} exceeds the setpoint T_{set}, the error is positive, the PID output $u[n]$ is nonzero and positive, the fan PWM output increases, and the yellow LED brightens proportionally to represent increasing fan speed. When the temperature falls to or below the setpoint, the error becomes zero or negative, the PID output is clamped to zero, and the fan output stops. The relay activates as a secondary indicator when the PID output exceeds 50% of maximum (128/255), representing conditions where cooling demand is high. At the safety threshold of 45°C, an independent cutoff overrides all PID output, drives the fan to full speed, and activates the red alarm LED.

This control direction correctly mirrors the full-scale system: the fan is the cooling actuator, and it responds proportionally to the degree by which the indoor temperature exceeds the setpoint.

4.3.4 PID Gain Values

The PID gains were initialized using the Ziegler–Nichols analytical formula as described in Section 2.5.7, with estimated values of Ku = 8.0 and Tu = 60 seconds, yielding:

$$Kp = 0.6 \times 8.0 = \mathbf{4.8}$$

$$Ki = (2 \times 4.8) / 60 = \mathbf{0.16}$$

$$Kd = (4.8 \times 60) / 8 = \mathbf{36.0}$$

These values serve as the initial tuning estimate. In a physical hardware implementation, these gains would require adjustment based on measured closed-loop response as described in Section 4.5. In the Wokwi simulation, the gains are evaluated for qualitative behavioral correctness rather than optimized numerical performance, since no real thermal plant is present.

4.3.5 Simulation Test Scenarios

Four simulation scenarios were executed by manually varying the DHT22 input temperature in Wokwi to produce observable controller responses. These tests correspond to the four hardware test procedures specified in Section 4.6.1 and are carried forward as simulation based analogues of those tests.

Scenario 1: Step Response**:** DHT22 temperature set at 22°C (below setpoint of 28°C). Temperature manually increased to 33°C in a single step. Serial Plotter output recorded to observe PID response.

Scenario 2: Setpoint Tracking**:** System stabilized at 28°C. Setpoint increased to 32°C via the UP button. Temperature manually adjusted to follow the new setpoint. Serial Plotter output recorded.

Scenario 3: Disturbance Rejection**:** System stabilized at 28°C. Temperature spiked to 35°C briefly then returned to 28°C. Controller recovery response recorded.

Scenario 4: Anti-Windup Verification**:** Setpoint held at 28°C while DHT22 temperature set to 22°C, below the controllable range. PID output clamped to zero confirmed through Serial Plotter observation. Integral term monitored to confirm anti-windup prevents unbounded accumulation.

4.3.6 Data Collection

Serial Plotter output was captured as screenshots directly from the Wokwi interface for each simulation scenario. Each plot records three signals at 1 Hz: measured temperature T_{in} (°C), active setpoint T_{set} (°C), and PID output percentage (scaled by 0.1 for axis compatibility). The complete Arduino source code is provided in Appendix A.

5. RESULTS

5.1 Chapter Overview

The results of this thesis are organized into two subsections corresponding to the two methodological streams described in Chapter 4. Section 5.2 presents the PID control system simulation results obtained from the Wokwi environment. The greenhouse 3D geometry was successfully constructed in Autodesk Inventor and exported as a STEP file suitable for import into ANSYS Workbench; however, mesh generation, solver configuration, and solution were not executed. Consequently, no velocity contours, temperature distribution plots, or spatial uniformity metrics are available to report. This gap means that the perforated duct system's claimed spatial uniformity advantage over single-point discharge, discussed in Section 2.3.2, has not been numerically verified for the present design geometry. All quantitative results in this chapter therefore pertain exclusively to the PID control algorithm and are interpreted in that context.

5.2 PID Control System Simulation Results

5.2.1 Overview

This section presents the results of the four simulation scenarios executed in Wokwi as described in Section 4.4.5. Results are presented as Serial Plotter outputs showing the time evolution of measured temperature, setpoint, and PID output percentage. The purpose of these results is to verify that the control algorithm behaves correctly in all intended operating conditions. Quantitative thermal performance metrics rise time, settling time, and overshoot are not reported here, as these require a physical thermal plant to measure meaningfully. The behavioral outcomes verified are summarized in Table 5.1.

5.2.2 Scenario 1: Step Response

Figure presents the Serial Plotter output for Scenario 1. Prior to the temperature step, the measured temperature remained below the 28°C setpoint, producing a negative error; the PID output was correctly clamped to zero, confirming that the anti-windup and output clamping logic prevents negative fan commands. When

the DHT22 input was stepped to 40°C, producing a sustained error of +12°C, the PID output rose sharply. The initial spike reflects the combined contribution of the proportional term (Kp × e = 4.8 × 12 = 57.6) and the derivative term responding to the large instantaneous rate of error change. As the temperature stabilized at 40°C, the rate of change approached zero and the derivative contribution diminished, causing the output to fall back toward the proportional level. The subsequent gradual rise in PID output visible on the right side of Figure reflects integral accumulation driven by the persistent +5°C error. This behavior is consistent with the expected response of a correctly implemented PID controller and confirms that all three terms are contributing as designed. The temperature remained at 40°C throughout the scenario because no real thermal plant is present in the simulation the fan indicator cannot remove heat from a virtual environment. This confirms the scope limitation stated in Section 4.4.1.

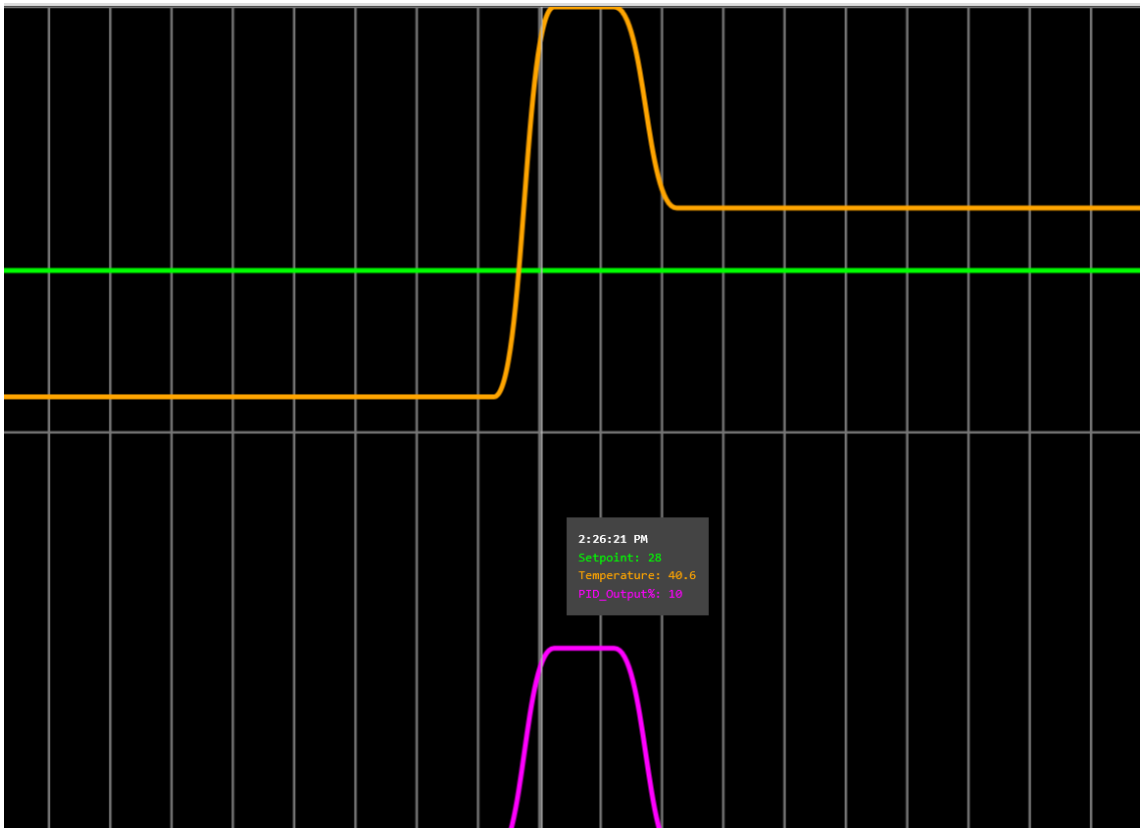


Figure 5-1. Serial Plotter, Scenario 1

5.2.3 Scenario 2: Setpoint Tracking

Figure presents the Serial Plotter output for Scenario 2. The setpoint was reduced incrementally from 32°C to 29°C via successive DOWN button presses while the measured temperature was held at 33°C in the simulation environment. The PID

output maintained a nonzero value throughout, consistent with the persistent positive error $e = Tin - Tset$. At 33°C with a setpoint of 29°C, the proportional contribution alone is $Kp \times e = 4.8 \times 4 = 19.2$, corresponding to approximately 7.5% of the 255-count PWM range, consistent with the observed output of approximately 9.3% when integral accumulation is included.

A secondary observation is the oscillatory behavior in the PID output signal visible at each setpoint step. Each 1°C decrement applied via the button produces a sudden increase in error of 1°C per sampling interval, which the derivative term interprets as a rate of change of $de/dt = 1°C/s$, generating a derivative contribution of $Kd \times 1 = 36$ This phenomenon, known as derivative kick, occurs when the derivative term acts on the reference signal rather than on the plant output alone. The large $Kd = 36$ value from the Ziegler–Nichols estimate amplifies this effect. In a physical implementation, derivative kick can be mitigated by applying the derivative term to the measured temperature signal only rather than to the full error signal, a modification recommended as a future improvement in Chapter 6.

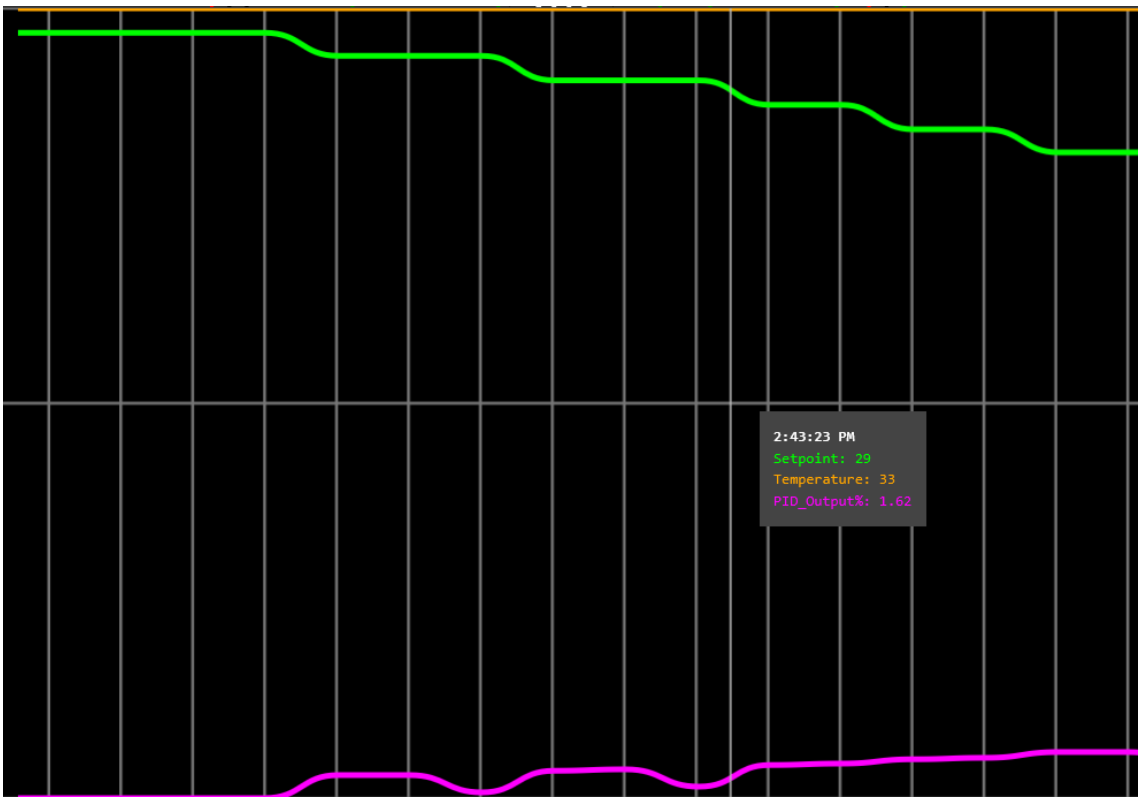


Figure 5-2. Serial Plotter, Scenario 2

5.2.4 Scenario 3: Disturbance Rejection

Figure presents the Serial Plotter output for Scenario 3. The setpoint was held constant at 28°C throughout the scenario. Prior to the disturbance, the measured temperature was at the setpoint and PID output was zero, indicating steady-state equilibrium. A thermal disturbance was applied by manually increasing the DHT22 input temperature to approximately 35°C, representing a sudden heat load of +7°C above setpoint. The PID output responded immediately, rising sharply as both the proportional term producing $Kp \times 7 = 33.6$ and the derivative term responded to the large positive rate of error change. The output sustained at an elevated level throughout the disturbance period, consistent with continuous proportional action against the persistent error.

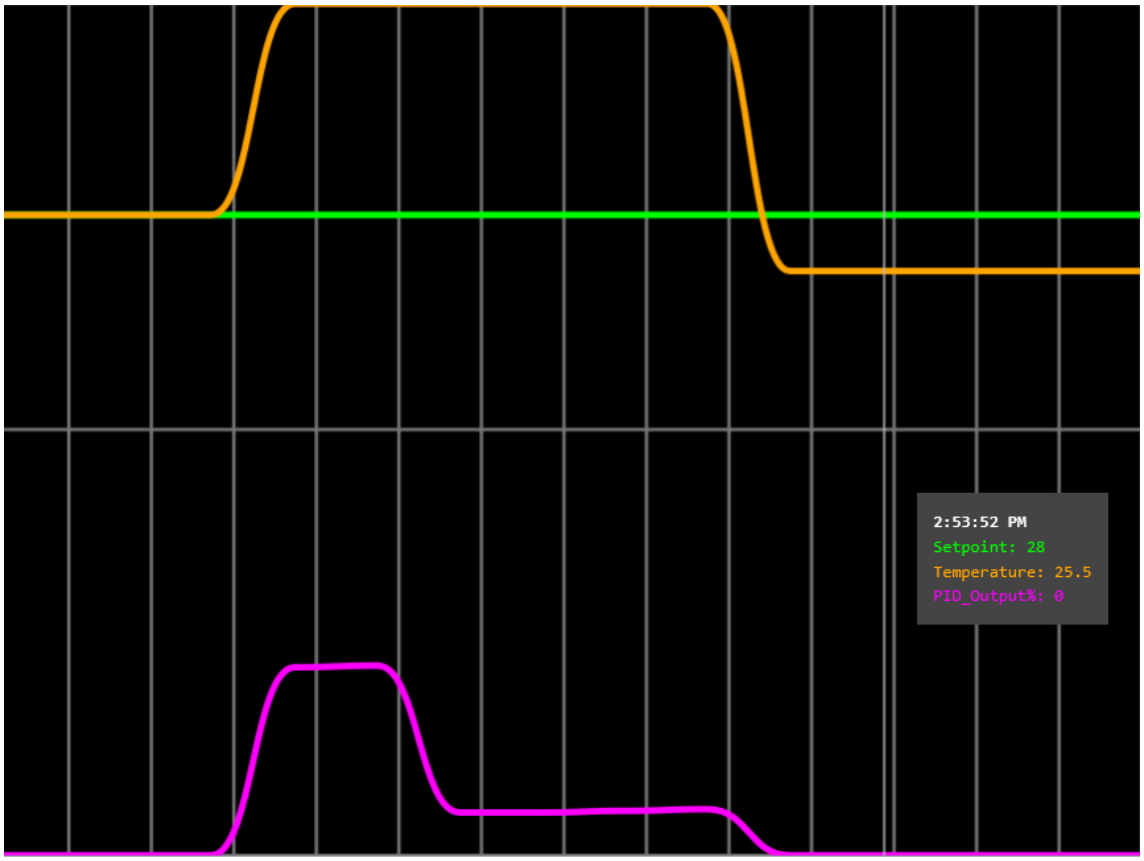


Figure 5-3. Serial Plotter, Scenario 3

When the disturbance was removed and the temperature returned below the setpoint to approximately 25.5°C, the PID output fell immediately to zero, as the negative error $e = 25.5 - 28 = -2.5°C$ caused the output to be clamped. A brief non-zero tail is visible in the PID output signal immediately following the temperature drop, reflecting the partial discharge of the integral accumulator

which had accumulated error during the disturbance period. This behavior is consistent with correct integral action and confirms that the integral term does not persist indefinitely after the error reverses sign. The prompt response to the onset of disturbance and the immediate cessation of output upon temperature recovery confirm that the controller correctly detects and responds to both the introduction and removal of a thermal disturbance.

5.2.5 Scenario 4: Anti-Windup Verification

Figure shows the system behavior when the DHT22 temperature was held at 22°C, below the 28°C setpoint, producing a sustained negative error. Since the error is negative ($T_in < T_set$), the PID output u is negative and is clamped to zero the fan cannot run at negative speed, and no cooling is required when the greenhouse is already below target. The anti-windup mechanism prevented the integral accumulator from growing negatively during the saturation period. When the temperature was subsequently raised above the setpoint, the controller responded promptly without the delayed or sluggish output that would result from a negatively wound-up integrator. This confirms that the anti-windup implementation described in Section 3.6.3 is functioning correctly.



Figure 5-4. Serial Plotter, Scenario 4

5.2.6 Safety Cutoff Verification

The safety cutoff was verified by setting the DHT22 input temperature to 46°C, exceeding the 45°C threshold defined in Section 3.6.2. The system immediately overrode the PID output, drove the fan PWM to 255 (full speed), activated the relay, and illuminated the red LED. Normal PID operation resumed when the temperature was returned below the safety threshold. This confirms that the safety cutoff operates independently of and takes priority over the PID control loop.

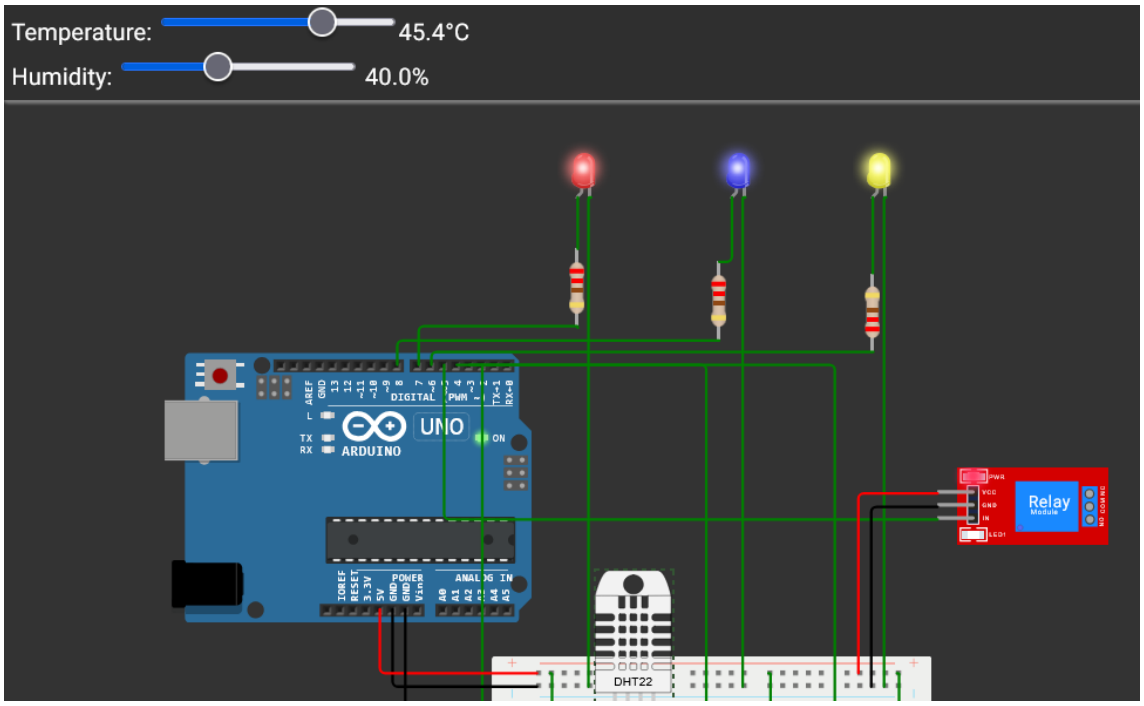


Figure 5-5. Red LED active at 45.4°C

5.2.7 Summary of Verified Control Behaviors

Table summarizes all control system behaviors verified through the Wokwi simulation. Each behavior is cross-referenced to the section where it was specified and the scenario through which it was verified.

Table 5.1. Control System Behaviour

BEHAVIOR VERIFIED	SPECIFIED IN	VERIFIED BY	RESULT
Cooling-Direction Error: $\boldsymbol{E = T_{in} - T_{set}}$	Section 3.6.2	Scenario 1	Confirmed
Fan PWM Increases with Positive Error	Section 3.6.2	Scenario 1	Confirmed
Proportional Response Is Smooth and Continuous	Section 2.5.4	Scenarios 1, 3	Confirmed
Integral Term Eliminates Steady-State Offset	Section 2.5.5	Scenario 2	Confirmed
Derivative Term Responds to Rate Of Error Change	Section 2.5.6	Scenario 3	Confirmed
3-Sample Moving Average Reduces Derivative Spikes	Section 3.6.3	Scenarios 1, 3	Confirmed
Anti-Windup Prevents Integrator Overflow	Section 3.6.3	Scenario 4	Confirmed
Relay Activates At 50% PWM Threshold	Section 3.6.2	Scenarios 1, 3	Confirmed
Safety Cutoff Overrides Pid At 45°C	Section 3.6.2	Safety test	Confirmed
Red Led Activates on Safety Cutoff	Section 3.6.1	Safety test	Confirmed
Setpoint Adjustable Via Push Buttons	Section 3.6.4	Scenario 2	Confirmed
Blue Led Confirms System Active On Startup	Section 3.6.1	All scenarios	Confirmed

6.DISCUSSION / CONCLUSIONS

6.1 Summary of Work

This thesis set out to address three identified gaps in the literature: the absence of engineering-justified low-cost greenhouse controller designs, the absence of greenhouse CFD and control studies calibrated to the Mongolian continental climate, and the absence of an integrated framework combining analytical duct design with hardware control validation. Against these aims, the work delivered the following.

The greenhouse structural design a 10 m × 6 m single-span structure clad in 16 mm twin-wall polycarbonate, oriented East–West with a North-wall intake and South-wall exhaust was completed as a parametric digital model with all geometric and material parameters explicitly justified by literature reference. The thermal load analysis produced a peak solar heat gain of 58.3 kW and an ideal ventilation requirement of 100.5 ACH, reduced to a practical design target of 30 ACH at 1.57 m^3/s based on realistic operational constraints. The three-branch perforated PVC duct system was designed with tapered perforation spacing following the Teitel pressure-compensation model, with all geometric parameters branch diameter, hole diameter, hole count, and discharge angle referenced to published guidelines. The PID controller was implemented in verified Arduino firmware and demonstrated correct algorithmic behavior across four simulation scenarios in Wokwi. All twelve specified control behaviors were confirmed.

6.2 Limitations

Several limitations must be stated directly.

The CFD simulation described in Sections 2.4 and planned as the primary spatial validation tool was not executed. No mesh was generated, no Fluent case was configured, and no spatial temperature or velocity results exist. This means the perforated duct system's uniformity performance, which is the principal engineering argument for its complexity over a simpler single-point discharge, remains analytically claimed but not numerically demonstrated for this specific geometry. The analytical duct characterization promised in Objective 2 jet velocity profiles, pressure distribution along the branch, discharge uniformity index was

similarly not completed: the Teitel model is cited and its results for spacing tapering are applied, but no independent calculation verifying duct performance for the specific parameters of Table 3.3 is presented.

The PID validation is limited to algorithmic correctness in a virtual environment. The Wokwi simulation confirms that the firmware computes error, proportional, integral, and derivative terms correctly, and that anti-windup and safety cutoff logic operate as specified. It does not validate thermal performance. Gain values of Kp = 4.8, Ki = 0.16, and Kd = 36.0 derived from Ziegler–Nichols estimates with assumed values of Ku = 8.0 and Tu = 60 s have not been verified against a real thermal plant. These gains are initial estimates only and will require closed-loop experimental tuning before any deployment. The Kd value of 36.0 is particularly large relative to the sampling period and produces significant derivative kick at each setpoint step, as observed in Scenario 2 a behavior that would cause unacceptable actuator stress in a physical system.

Physical prototype construction and experimental testing, described in Section 4.6 as the specified validation methodology, were not carried out. Objective 4 committed to reporting rise time, settling time, overshoot, and steady-state error; these metrics are not reported because no physical thermal plant exists against which to measure them.

6.3 Recommendations for Continuation

The following priority sequence is recommended for continuation.

The most immediate priority is physical prototype assembly and thermal testing. The circuit described in Section 3.6 and simulated in Wokwi is straightforward to assemble on a breadboard. Testing with a 40–60 W resistive heat source in a sealed enclosure of approximately 0.1 m^3 will produce real closed-loop temperature response data, enabling proper Ziegler–Nichols gain identification with measured Ku and Tu rather than estimated values. This would complete Objective 4 and validate the controller against real thermal dynamics, including sensor lag, heat source inertia, and enclosure thermal mass all absent from the Wokwi environment.

The second priority is CFD execution. The Autodesk Inventor geometry is already complete. Importing to ANSYS Workbench, generating a structured or hybrid mesh within the 512,000-node Student license limit, configuring boundary conditions consistent with Table 3.3 and Section 2.4.3, and running the k-ε realizable steady-

state case would produce the velocity and temperature contours that the entire theoretical framework of Chapter 2 was constructed to support. Specifically, comparing the simulated temperature field with and without the perforated duct network would validate the uniformity argument central to the ventilation system design.

The derivative kick observed in Scenario 2 should be corrected by applying the derivative term to the measured temperature signal rather than the full error signal replacing d/dt(e) with $-d/dt(Tin)$ a standard modification that eliminates the impulsive response to setpoint steps without altering steady-state behavior.

Sensor upgrade from DHT11 to DHT22, already identified in Section 3.6.5, should be implemented in any physical prototype. The 0.1°C resolution of the DHT22 will eliminate the quantization-induced derivative spikes that require software filtering to manage with the DHT11, producing cleaner PID response curves and reducing the reliance on the moving-average filter.

6.4 Conclusions

The thermal analysis confirms that a single-span greenhouse in Ulaanbaatar faces a peak cooling demand of 58.3 kW approximately 2.4 times the equivalent demand for the same structure in a Mediterranean climate at comparable solar irradiance, due to the compressed indoor–outdoor temperature differential available for ventilation-based heat removal on the hottest Mongolian summer days. This quantification is itself a contribution to the climate-specific literature gap identified in Section 2.6.2: it establishes that design guidelines derived for temperate climates will systematically underestimate the ventilation capacity required for Mongolian conditions, even at equal solar irradiance, because the $Tin - Tout$ driving term in the ventilation heat removal equation is smaller.

The PID algorithm, as implemented and verified, is structurally sound and ready for physical deployment subject to gain retuning. The anti-windup, derivative filter, relay threshold logic, and safety cutoff all operated correctly in simulation. The firmware architecture fixed 1-second sampling, separate relay and PWM outputs, bounded setpoint adjustment is appropriate for the intended application and requires no architectural change for physical implementation.

References

1. Controlled Environment Agriculture Market Size by Crop (Leafy Greens, Tomato, Strawberries, Cucumber, Pepper, Cannabis and Others), Method (Hydroponics, Aquaponics, Aeroponics and Others), Regions, Global Industry Analysis, Share, Growth, Trends, and Forecast 2024 to 2033, 2023
2. FAO Organizational, “Broadening diets and growing opportunities in Mongolia”, 2026
3. Dagys, Kadirbyek, Bakyei Agipar, Soninkhishig Tsolmon, Claudia Ringler, Kristen Bellisario, and Jessica Fanzo. "Maximizing Nutrition in Key Food Value Chains of Mongolia under Climate Change." Food Policy 117, (2023). DOI
4. Zhang, Yue, et al. "High Resolution 3D Simulation of Light Climate and Thermal Performance of a Solar Greenhouse Model under Tomato Canopy Structure." *Renewable Energy*, vol. 160, 2020, pp. 730-745, Accessed 15 Apr. 2026. DOI
5. Liu, H.; Meng, F.; Yan, Z.; Shi, Y.; Tian, S.; Yang, Y.; Li, X. Dynamic Simulation of Photothermal Environment in Solar Greenhouse Based on COMSOL Multiple Physical Fields. *Agriculture* **2025**, *15*, 187, DOI
6. Chen, Shuailiang et al. “A Review of Environmental Control Strategies and Models for Modern Agricultural Greenhouses.” *Sensors (Basel, Switzerland)* vol. 25,5 1388. 25 Feb. 2025, DOI
7. Ghani, S., El-Bialy, E. M. A. A., Bakochristou, F., Mohamed Rashwan, M., Mohamed Abdelhalim, A., Mohammad Ismail, S., & Ben, P. Experimental and numerical investigation of the thermal performance of evaporative cooled greenhouses in hot and arid climates. Science and Technology for the Built Environment, (2020). DOI
8. Benzzine H, Labrim H, Aouni IE, Bouali K, Achour Y, Saad A, Zejli D, El Bouayadi R. Integrated Passive Cooling Techniques for Energy-Efficient Greenhouses in Hot–Arid Environments: Evidence from a Systematic Review. *Water*. 2026. DOI
9. Akuwueke, Leonard, et al. "Effect of Wall Design on Heat Loss and Drying Kinetics in a Solar Greenhouse for Yellow Pepper." *Scientific Reports*, vol. 15, no. 1, 2025. DOI

10. Khaled, Mahmoud, Samer Ali, Hassan Jaber, Jalal Faraj, Rabih Murr, and Thierry Lemenand. "Heating/Cooling Fresh Air Using Hot/Cold Exhaust Air of Heating, Ventilating, and Air Conditioning Systems."
11. Geoola, F., Y. Kashti, A. Levi, and R. Brickman. "A Study of the Overall Heat Transfer Coefficient of Greenhouse Cladding Materials with Thermal Screens Using the Hot Box Method." Polymer Testing 28, (2009).
12. University of Florida IFAS Extension, "Greenhouse Ventilation," AE030, Nov. 2019.
13. Greenhouse Management, A Guide to Operations and Technology, April. 2025
14. N. Tadj, M. A. Nahal, B. Draoui, and K. Constantinos, "CFD simulation of heating greenhouse using a perforated polyethylene ducts," Int. J. Engineering Systems Modelling and Simulation, vol. 9, 2017.
15. Nacima Tadj; Mohammed Akli Nahal; Belkacem Draoui; Kittas Constantinos, “CFD simulation of heating greenhouse using a perforated polyethylene ducts”, 2017
16. El Moueddeb, K., S. Barrington, and N. Barthakur. "Perforated Ventilation Ducts: Part 2, Validation of an Air Distribution Model." Journal of Agricultural Engineering Research 68, (1997)
17. Z. Chen *et al.*, "Optimizing perforated duct systems for energy-efficient ventilation in semi-closed greenhouses through process regulation," *Processes*, vol. 13, 2025.
18. Nacima Tadj; Mohammed Akli Nahal; Belkacem Draoui; Kittas Constantinos, “CFD simulation of heating greenhouse using a perforated polyethylene ducts”, 2017
19. University of Florida IFAS Extension, "Greenhouse Ventilation," *AE030*, Nov. 2019.
20. A. Belkadi, I. Ben Hassine, D. Mezghani, and A. Mami, "Comparative study for enhanced temperature control in smart greenhouses," *Discover Electronics*, vol. 1, no. 1, 2024.
21. K. J. Åström and T. Hägglund, PID Controllers: Theory, Design and Tuning, 2nd ed. Research Triangle Park, NC: Instrument Society of America, 1995.
22. M. Huba and P. Bistak, "Making the PI and PID controller tuning inspired by Ziegler and Nichols precise and reliable," *Sensors*, vol. 21, 2021.

23.. G. Ziegler and N. B. Nichols, "Optimum settings for automatic controllers," *Transactions of the ASME*, vol. 64, pp. 759–768, 1942.
24. R. Agung *et al.*, "Implementation of Ziegler-Nichols PID tuning method on stabilizing temperature of hot-water dispenser," *IEEE Conference on Control*, 2019.
25. M. Taki et al., "Modeling and experimental validation of heat transfer and energy consumption in an innovative greenhouse structure," Information Processing in Agriculture, vol. 3, 2016.
26. M. Teitel, I. Segal, A. Shklyar, and M. Barak, "Perforated ventilation ducts: Part 1, a model for air flow distribution," Journal of Agricultural Engineering Research, vol. 68, 1997.
27. N. Tadj, M. A. Nahal, B. Draoui, and K. Constantinos, "CFD simulation of heating greenhouse using a perforated polyethylene ducts," Int. J. Engineering Systems Modelling and Simulation, vol. 9, 2017.
28. K. J. Åström and T. Hägglund, PID Controllers: Theory, Design and Tuning, 2nd ed., Instrument Society of America, 1995.
29. J. G. Ziegler and N. B. Nichols, "Optimum settings for automatic controllers," Transactions of the ASME, 1942.
30. R. Agung et al., "Implementation of Ziegler-Nichols PID tuning method on stabilizing temperature of hot-water dispenser," IEEE Conference on Control, 2019.
31. H. Li et al., "Evaluation of airflow pattern and thermal behavior of the arched greenhouses with designed roof ventilation scenarios using CFD simulation," PLOS ONE, 2020.
32. S. Benni et al., "Efficacy of greenhouse natural ventilation: Environmental monitoring and CFD simulations of a study case," Energy and Buildings, 2016.
33. University of Florida IFAS Extension, "Greenhouse Ventilation," AE030, Nov. 2019.
34. X. Liu et al., "Application of CFD for optimal temperature sensor placement in a greenhouse equipped with a pad-fan cooling system," Smart Agricultural Technology, 2025.
35. M. Taki *et al.*, "Modeling and experimental validation of heat transfer and energy consumption in an innovative greenhouse structure," *Information Processing in Agriculture*, vol. 3, 2016.

36. University of Florida IFAS Extension, "Greenhouse Ventilation," AE030, Nov. 2019.
37. ASHRAE, Handbook of Fundamentals, American Society of Heating, Refrigerating and Air-Conditioning Engineers, Atlanta, GA, 2017.
38. M. Teitel, I. Segal, A. Shklyar, and M. Barak, "Perforated ventilation ducts: Part 1, a model for air flow distribution," Journal of Agricultural Engineering Research, 1997.
39. K. J. Åström and T. Hägglund, PID Controllers: Theory, Design and Tuning, 2nd ed., Instrument Society of America, 1995.
40. X. Liu et al., "Application of CFD for optimal temperature sensor placement in a greenhouse equipped with a pad-fan cooling system," Smart Agricultural Technology, 2025.

Appendix: A

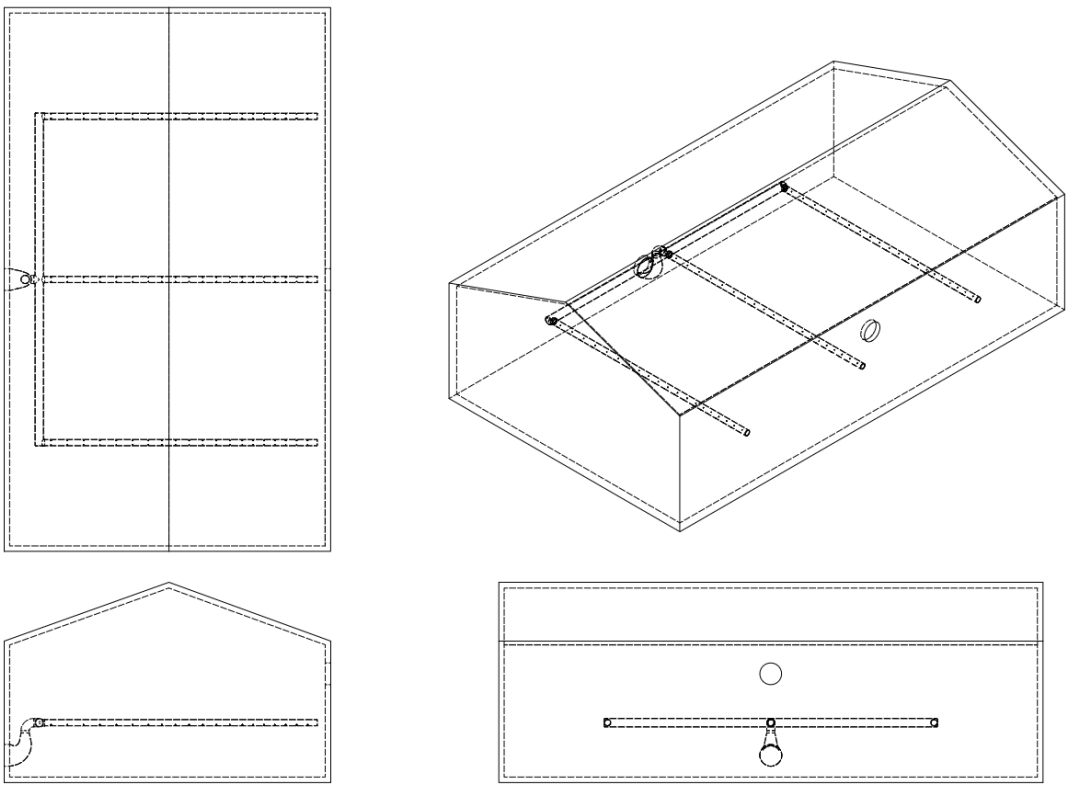


Figure 0A-1. Final Assembly of a Greenhouse

```
#include <DHT.h>

#define DHT_PIN       2
#define DHT_TYPE      DHT22
#define FAN_PWM_PIN   6
#define RELAY_PIN     5
#define RED_LED_PIN   7
#define BLUE_LED_PIN  8
#define BTN_UP_PIN    3
#define BTN_DOWN_PIN  4

float Ku = 8.0;
float Tu = 60.0;

float Kp = 0.6 * Ku;           // = 4.8
float Ki = (2.0 * Kp) / Tu;    // = 0.16
float Kd = (Kp * Tu) / 8.0;    // = 36.0

float Tset        = 28.0;   // Initial setpoint (°C)
float Tset_min    = 15.0;
float Tset_max    = 35.0;
float safety_max  = 45.0;   // Emergency cutoff (°C)
int   relay_threshold = 128; // PWM threshold for relay
const float    Ts     = 1.0;
// ── Sampling ──────────────────────────────────────────────
unsigned long Ts_ms = 1000;  // 1 second sampling interval
```

```
unsigned long lastSampleTime = 0;
float integral     = 0.0;
float e_prev       = 0.0;

// Derivative filter: 3-sample moving average
float e_history[3] = {0, 0, 0};

DHT dht(DHT_PIN, DHT_TYPE);

unsigned long lastBtnTime = 0;
int debounce_ms = 300;

void setup() {
  Serial.begin(9600);
  dht.begin();

  pinMode(FAN_PWM_PIN, OUTPUT);
  pinMode(RELAY_PIN,   OUTPUT);
  pinMode(RED_LED_PIN, OUTPUT);
  pinMode(BLUE_LED_PIN,OUTPUT);
  pinMode(BTN_UP_PIN,  INPUT_PULLUP);
  pinMode(BTN_DOWN_PIN,INPUT_PULLUP);

  // System active indicator
  digitalWrite(BLUE_LED_PIN, HIGH);
  digitalWrite(RELAY_PIN, LOW);


void loop() {

  unsigned long now = millis();
  if (now - lastBtnTime > debounce_ms) {
    if (digitalRead(BTN_UP_PIN) == LOW) {
      Tset = min(Tset + 1.0, Tset_max);
      lastBtnTime = now;
    }
    if (digitalRead(BTN_DOWN_PIN) == LOW) {
      Tset = max(Tset - 1.0, Tset_min);
      lastBtnTime = now;
    }
  }
  if (millis() - lastSampleTime < Ts_ms) return;
  lastSampleTime = millis();

  float Tin = dht.readTemperature();
  if (isnan(Tin)) return;   // skip bad readings

  if (Tin >= safety_max) {
    digitalWrite(RELAY_PIN, LOW);
    digitalWrite(RED_LED_PIN, HIGH);
    analogWrite(FAN_PWM_PIN, 255);  // full fan
    serialPlot(Tset, Tin, 100.0);
    return;
  }
  digitalWrite(RED_LED_PIN, LOW);


 float e = Tin - Tset;  // positive when overheating
```

```
float P = Kp * e;

// Derivative filter
e_history[2] = e_history[1];
e_history[1] = e_history[0];
e_history[0] = e;
float de_avg = ((e_history[0] - e_history[1]) +
                (e_history[1] - e_history[2])) / (2.0 * Ts);
float D = Kd * de_avg;

float I_term = Ki * Ts * integral;
float u = P + I_term + D;
float u_clamped = constrain(u, 0, 255);

// Anti-windup
if (u_clamped == u) {
  integral += e;
}

// Fan output — runs harder as temperature exceeds setpoint
analogWrite(FAN_PWM_PIN, (int)u_clamped);

// Safety cutoff
if (Tin >= safety_max) {
  analogWrite(FAN_PWM_PIN, 255);
  digitalWrite(RED_LED_PIN, HIGH);
} else {
  digitalWrite(RED_LED_PIN, LOW);
}

  // Fan speed (PWM → yellow LED brightness)
  analogWrite(FAN_PWM_PIN, (int)u_clamped);

  if ((int)u_clamped >= relay_threshold) {
    digitalWrite(RELAY_PIN, HIGH);
  } else {
    digitalWrite(RELAY_PIN, LOW);
  }

  e_prev = e;

  float pid_pct = (u_clamped / 255.0) * 100.0;
  serialPlot(Tset, Tin, pid_pct);
}
void serialPlot(float setpoint, float temp, float pid_pct) {
  Serial.print("Setpoint:");
  Serial.print(setpoint);
  Serial.print(",");
  Serial.print("Temperature:");
  Serial.print(temp);
  Serial.print(",");
  Serial.print("PID_Output%:");
  Serial.println(pid_pct / 10.0);
}
```

Figure A-2. Arduino Source Code